Information from Radio Observations and the First Results From the Murchison Widefield Array

Divya Oberoi
NCRA-TIFR

Rohit Sharma (NCRA)
Akshay S (IISER, Pune)
Sanjay Bhatnagar (NRAO)
Colin Lonsdale, Lynn Matthews, Victor Pankratius, Brian Timar (MIT Haystack)
Iver Cairns (Sydney University)
Randall Wayth (Curtin University)
Mihir Arjuwadkar (CMS, Pune University)

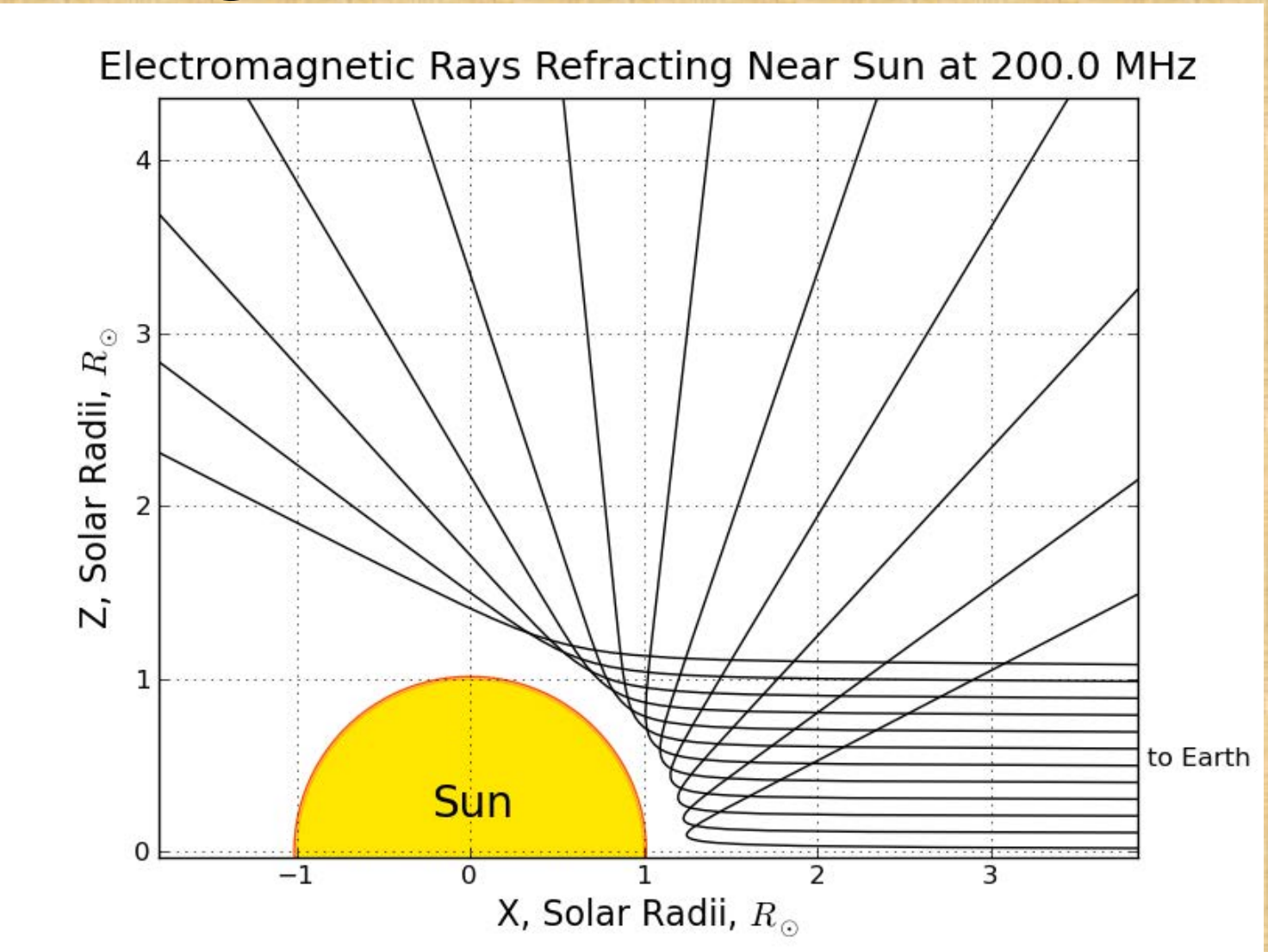
Members of the MWA Team

Outline

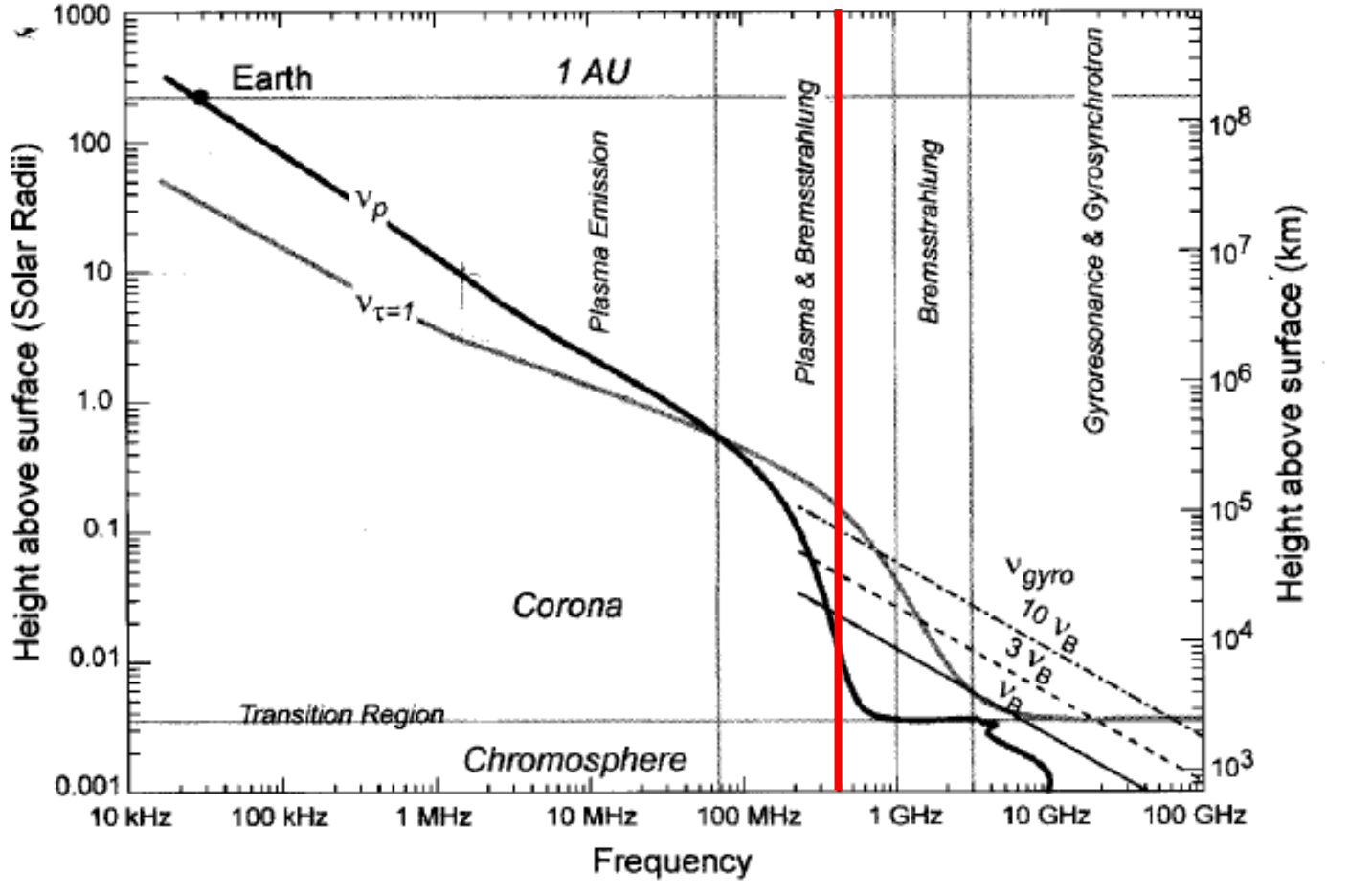
- Information from solar radio observations
  - Mechanisms
  - Examples
- What are we up against?
- What sort of an instrument does one need to study the Sun?
- Some representative MWA observations of the Sun

Background Thermal Emission

- L
  -
  -
- B



Characteristic frequencies and emission mechanisms



Plasma freq.
$\nu_p \approx 9 \times 10^3\ N_e^{1/2}$

Free-free emission
$\nu(\tau_{ff} = 1) \approx 0.5\ N_e\ T_e^{-3/4}\ L^{1/2}$

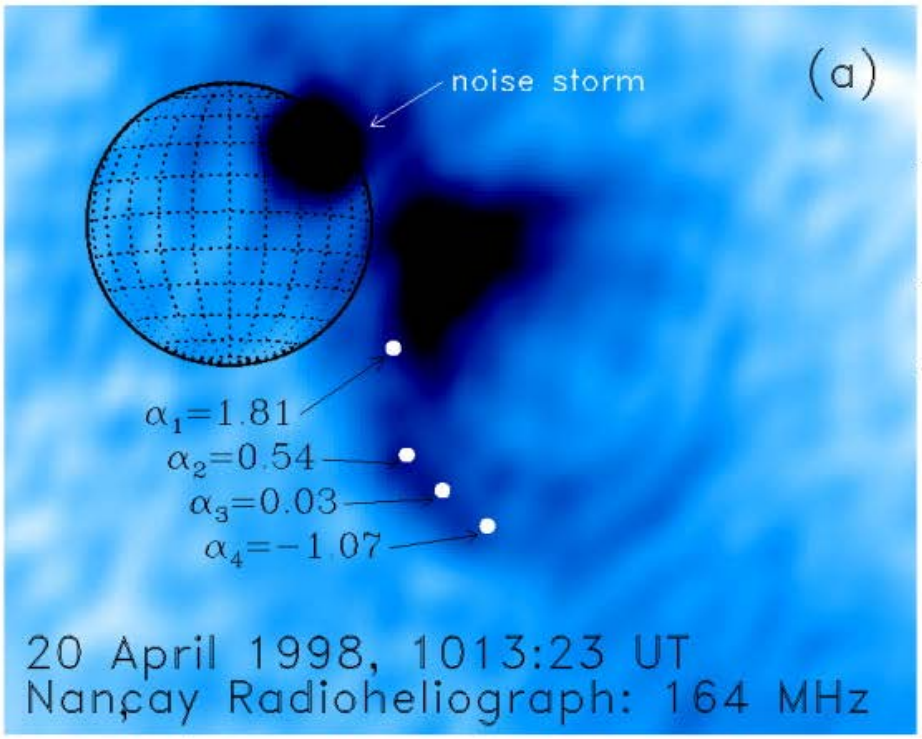
e gyro freq
$\nu_B \approx 2.8 \times 10^6\ B$

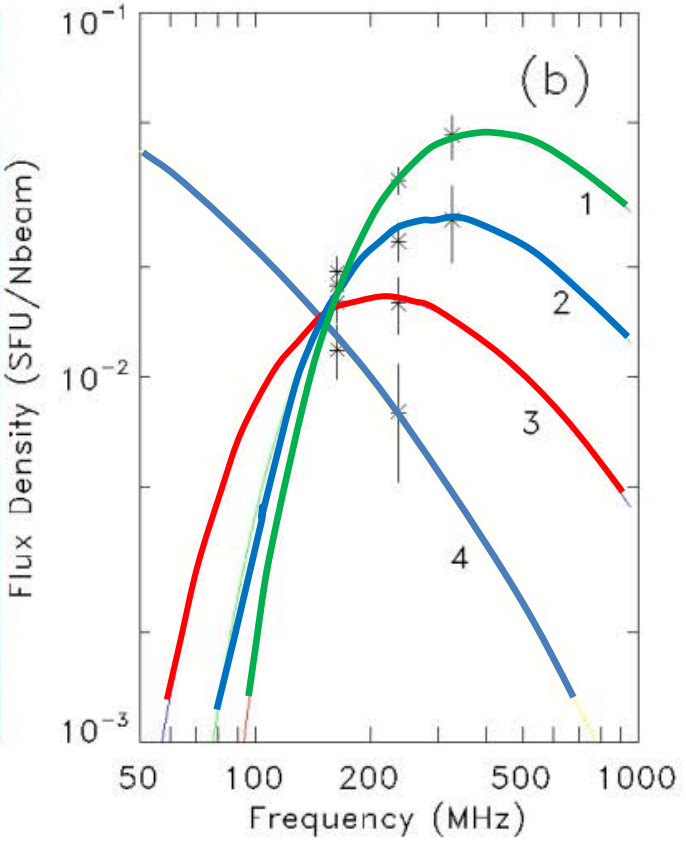
Gary and Hudson, 2007

For the Active Sun

- Incoherent emission mechanisms
  - Bremsstrahlung, Gyrosynchrotron
  - T_B contains all the physics (N_e, T_e, B field)
- Coherent emission mechanisms
  - Plasma emission (at fundamental and harmonic)
  - T_B – rate of growth of the instability
  - Properties in the freq-time plane, polarisation and morphology provide the physics

Gyrosynchrotron Emission



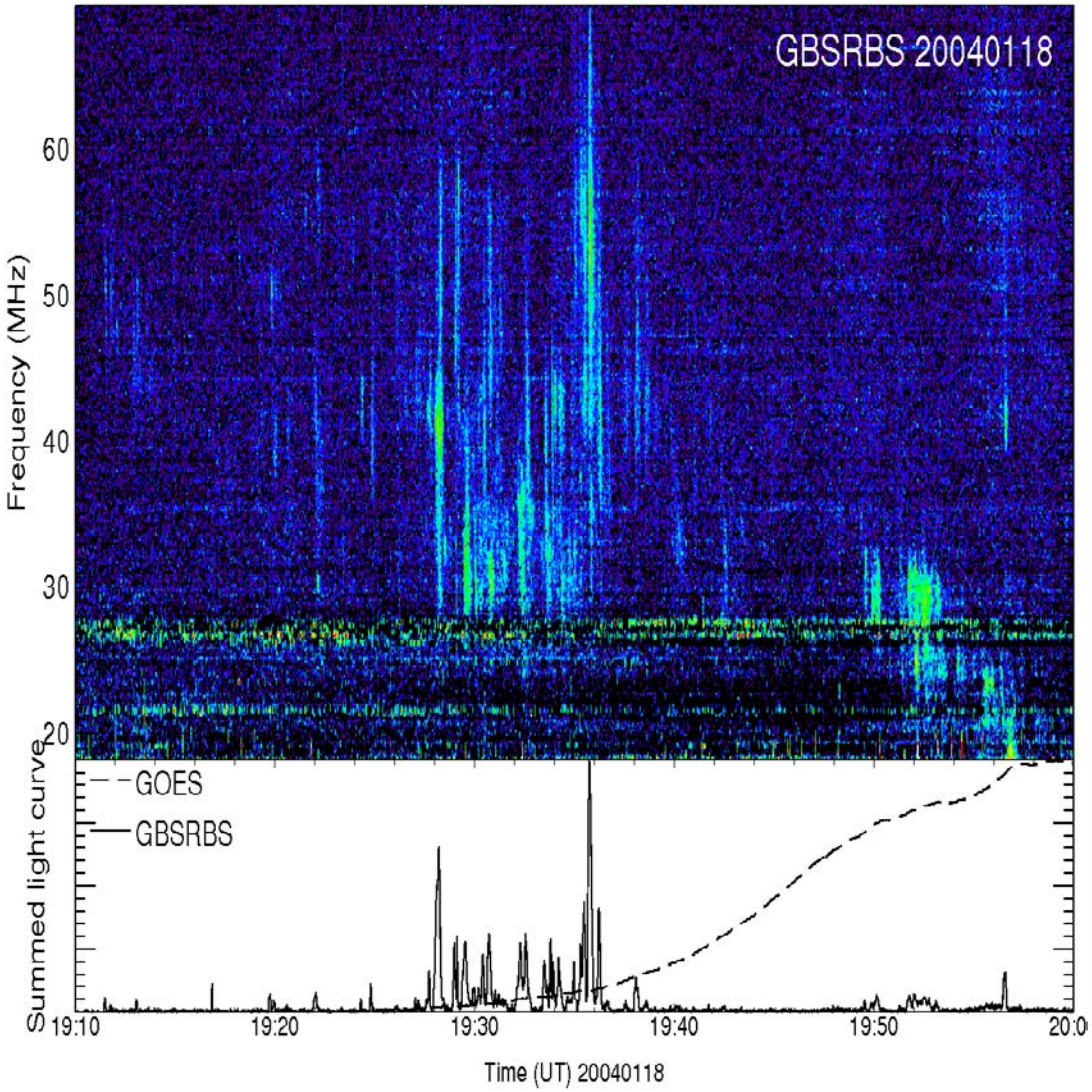


Bastian et al., 2001, ApJ

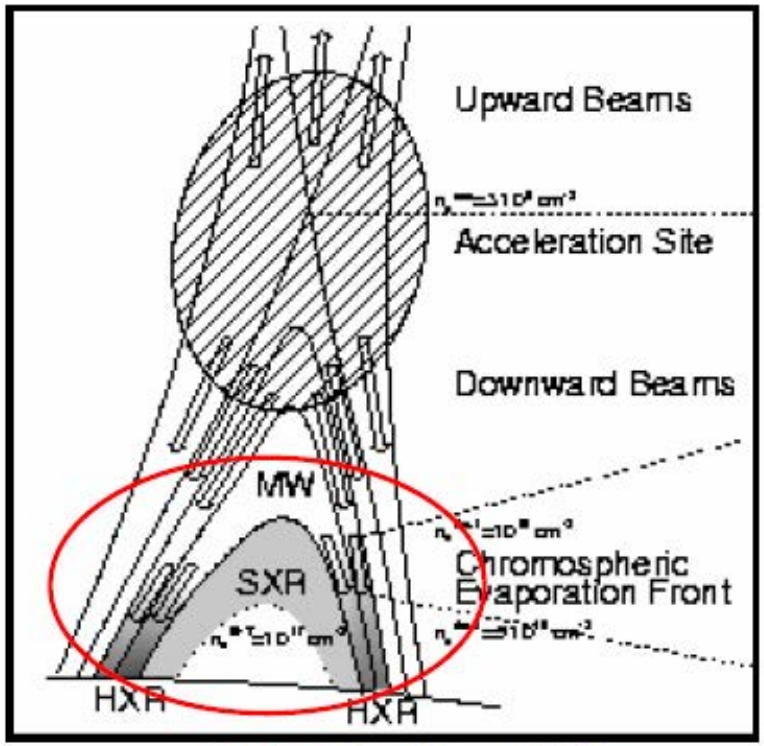
Optically thin gyrosynchrotron

- 0.5-5 MeV electrons trapped in expanding magnetic loops
- Invoke Razin-Tsytovich suppression to account for spectral inversion in low corona

Type III scenario



Long duration flare observed on west limb by Yohkoh and the Nobeyama radioheliograph on 16 March 1993.



Aschwanden & Benz 1997

Spatio-temporal correlation HXR, EUV, Radio

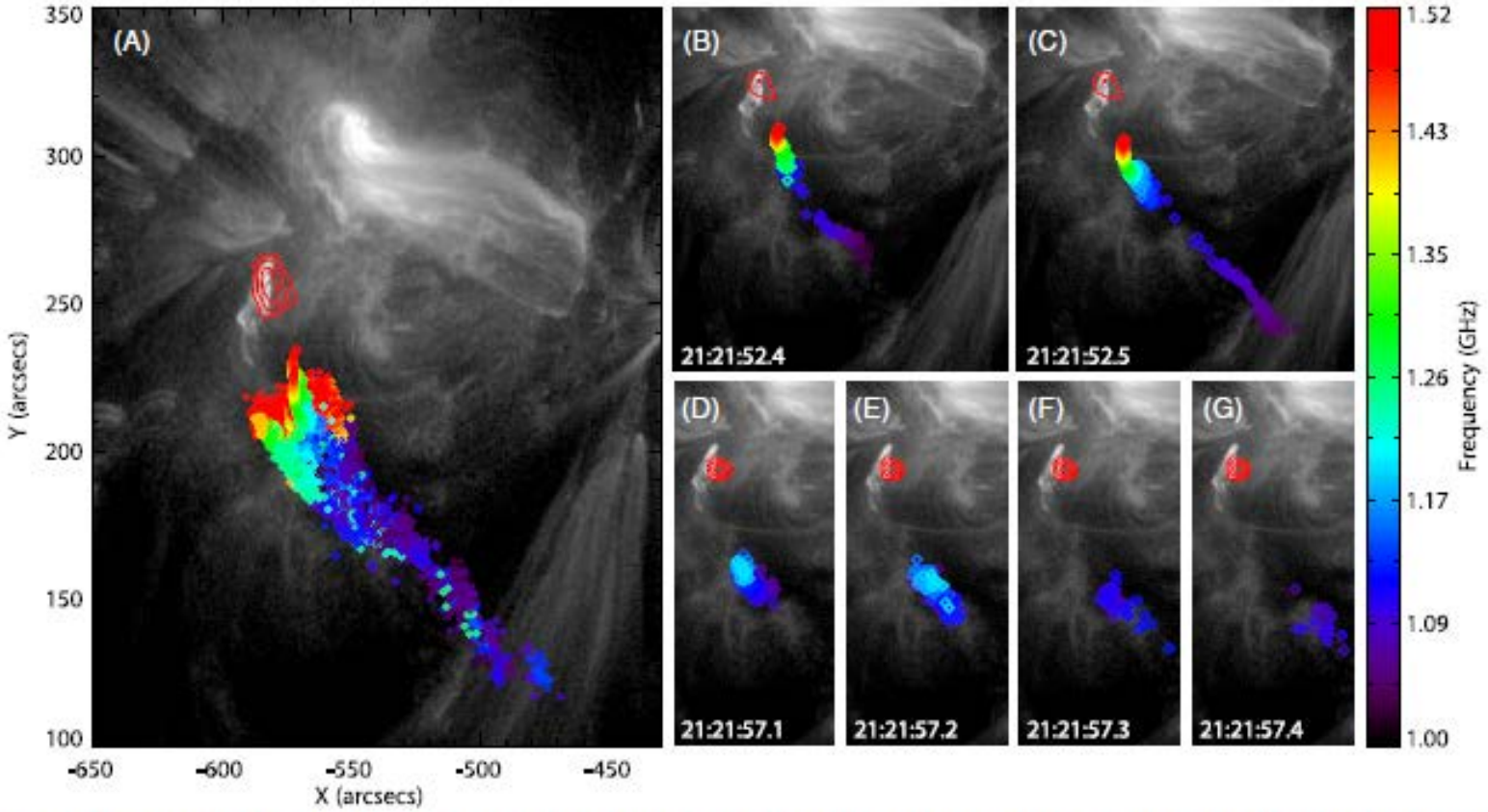


Figure 3. (A) Emission centroids of all type IIIdm bursts observed from 21:20:30 to 21:22:10 UT, colored from blue to red in increasing frequencies, showing electron beam trajectories in projection. Background is the *SDO*/AIA 131 Å image at 21:22:09 UT. Red contours are the 12 s integrated 12–25 keV HXR emission during the second HXR peak (around 21:21:50 UT). Emission centroids of a temporally resolved type IIIdm burst observed from 21:21:52.4 to 21:21:52.6 UT (shown by arrow "1" in Figure 1(H)) are shown by (B–C) for two successive 100 ms integrations. Another temporally resolved type IIIdm burst from 21:21:57.1 to 21:21:57.5 UT (arrow "2" in Figure 1(H)) is shown by (D–G) for four successive 100 ms integrations. Red contours are the 12–25 keV HXR source with a 4 s integration closest to the type-IIIdm-burst times.

Chen et al., ApJ, 763:L21, 2013

Gauribidanur Group

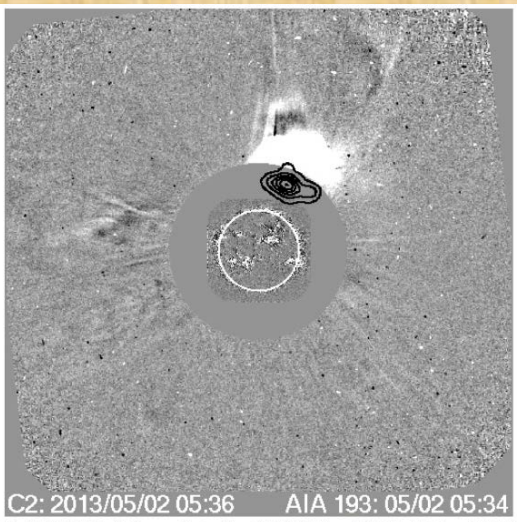


Figure 4. Composite of the 80 MHz GRAPH radioheliogram of the type II burst (05:08 UT) in Figure 1, *SDO*-AIA 193 Å image (≈05:34 UT), and *SOHO*-LASCO C2 image (≈05:36 UT) obtained on 2013 May 2. The peak T_b of the radioheliogram is $\approx 3.7 \pm 0.3 \times 10^9$ K and the contours are in interval of 10% of the peak T_b. The white circle (radius = $1R_\odot$) at the center indicates the solar limb. The larger, concentric gray circle (radius $\approx 2.2R_\odot$) represents the occulting disk of the *SOHO*-LASCO C2 coronagraph. Solar north is straight up and solar east is to the left in the image. The enhanced emission above the northwest quadrant of the coronagraph occulting disk corresponds to the white light CME discussed in the text.

- Observations of a Type II burst associated with a CME
- Estimates of B ahead and behind the CME, in the range of 0.3-2 G at ~2 R_{sun}

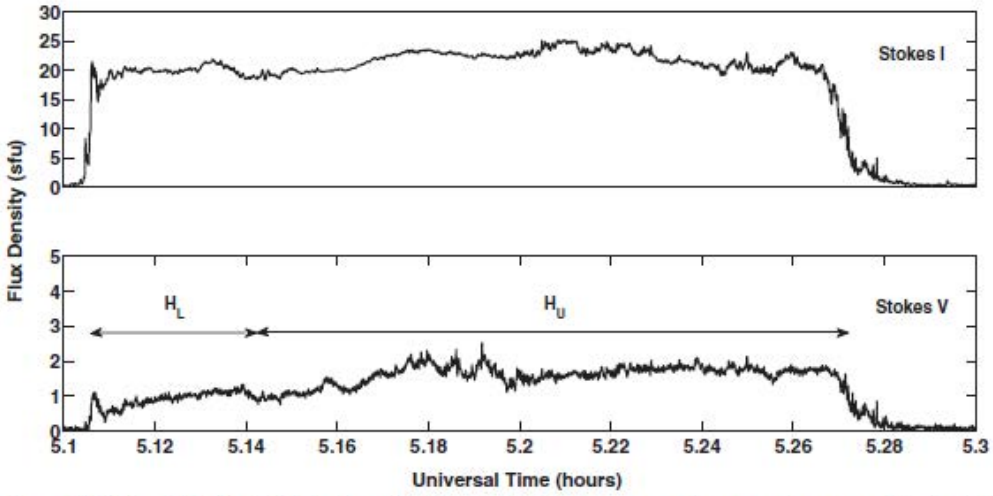
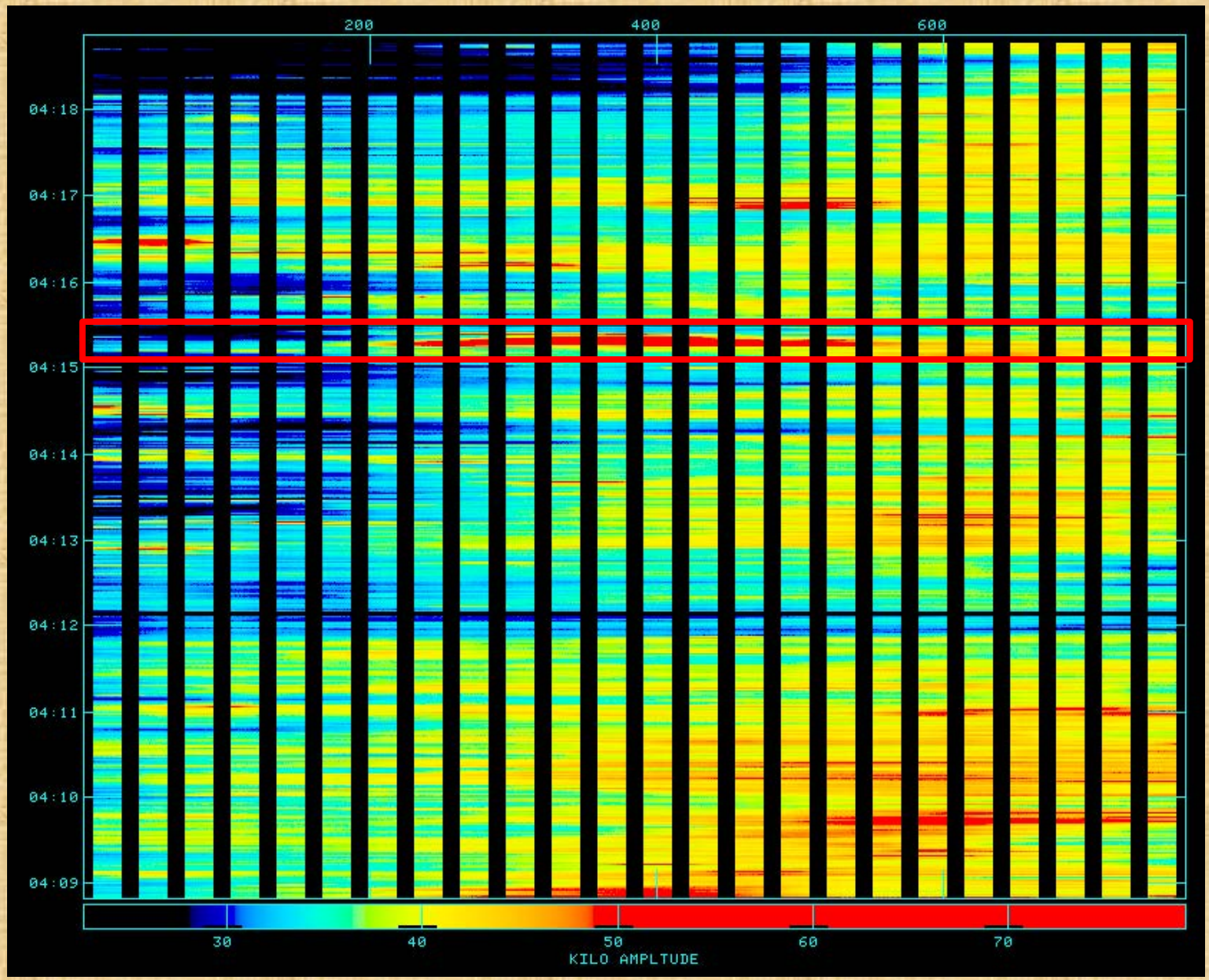


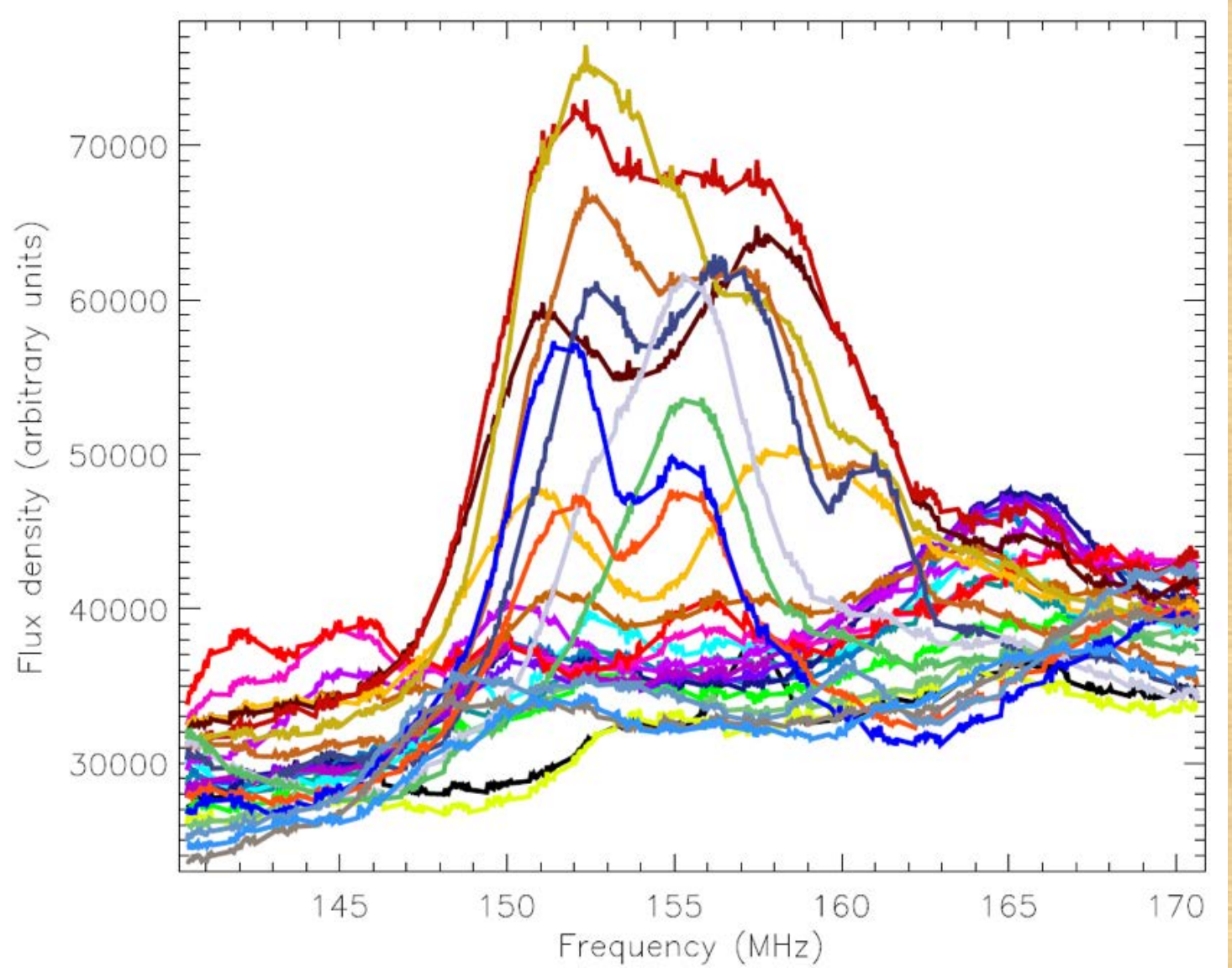
Figure 6. GRIP observations at 80 MHz on 2013 May 2 during the period 05:06–05:18 UT. The upper and lower panels correspond to the Stokes *I* and *V*, respectively. There is noticeable circularly polarized emission during the corresponding 80 MHz type II burst period in Figure 1.

Hariharan et al., 795, 14, 2014



25 Sep, 2011, 140.2-170.9 MHz, ~4:09-4:19 UT, auto-correlation, Amp, X pol

Extreme Variability



Solar Imaging Requirements

- Extreme time variability
- Spectral features over small fractional bandwidths
- Emission scales – resolution/scattering limit to ~45’
- Dynamic range requirements $\geq 10^5$
- *High dynamic range, high fidelity spectroscopic snapshot imaging capability over a wide band.*

Murchison Widefield Array



N. Hurley-Walker (Curtin)


Murchison

Antennas



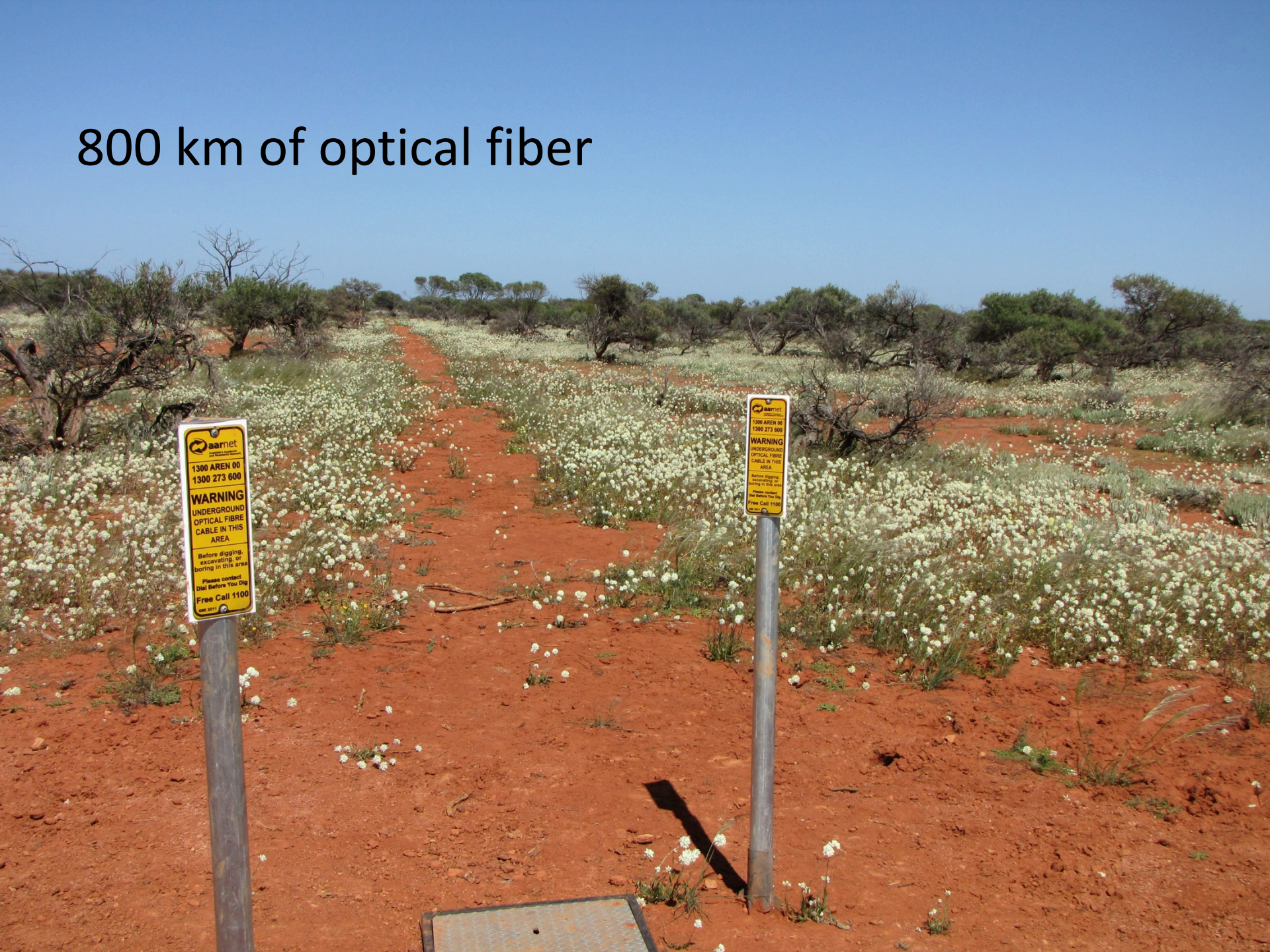
Receivers



Central Signal Processing



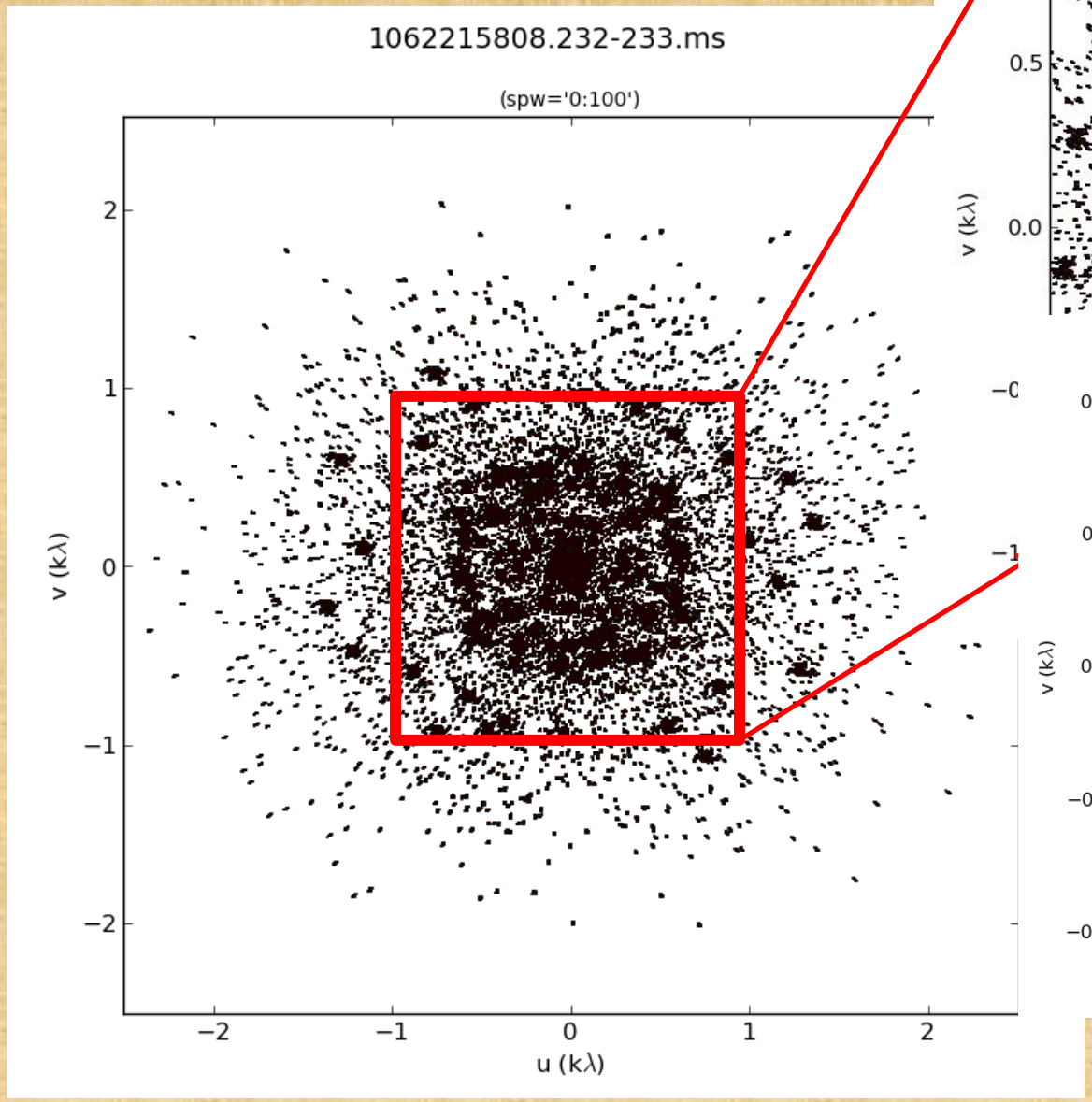
800 km of optical fiber

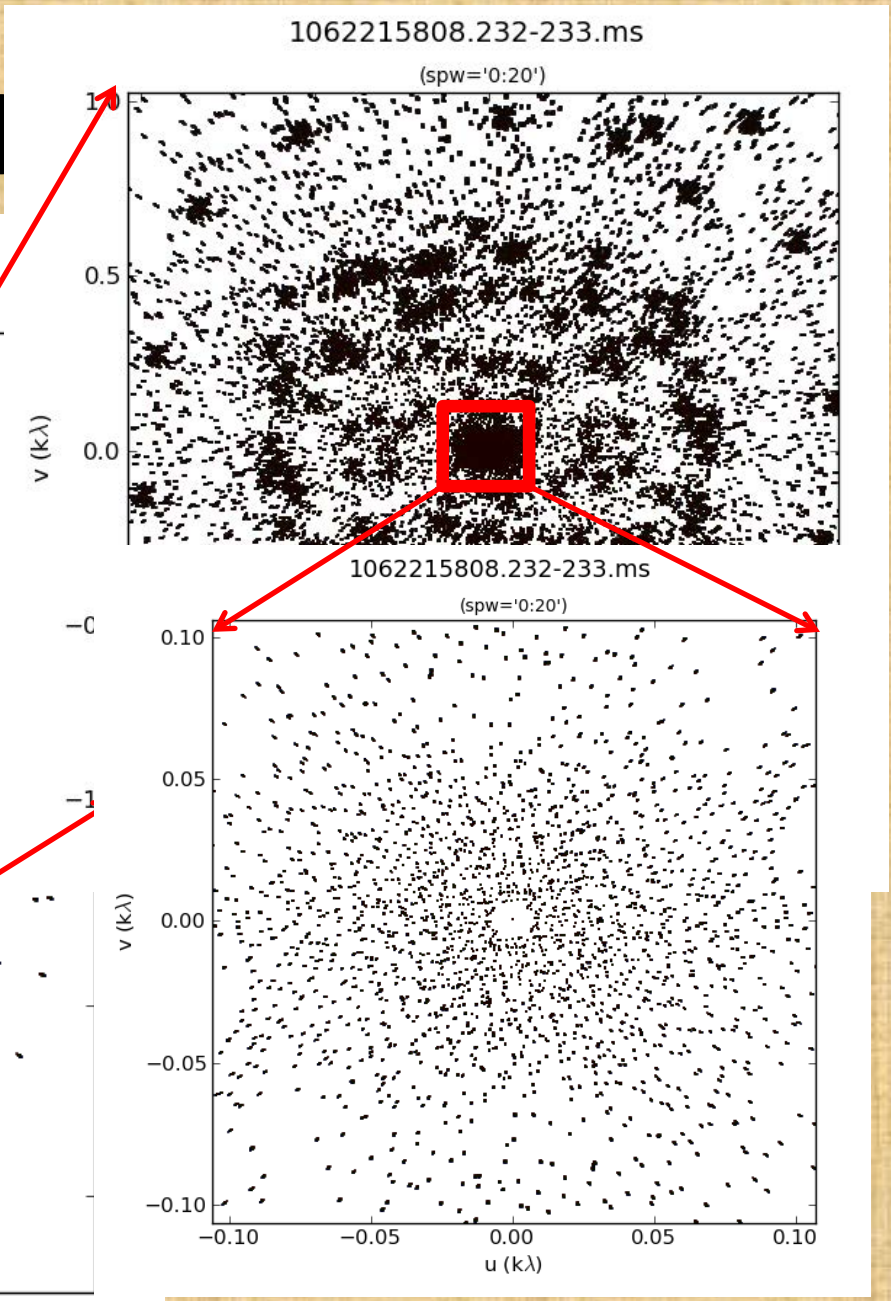


Pawsey Centre



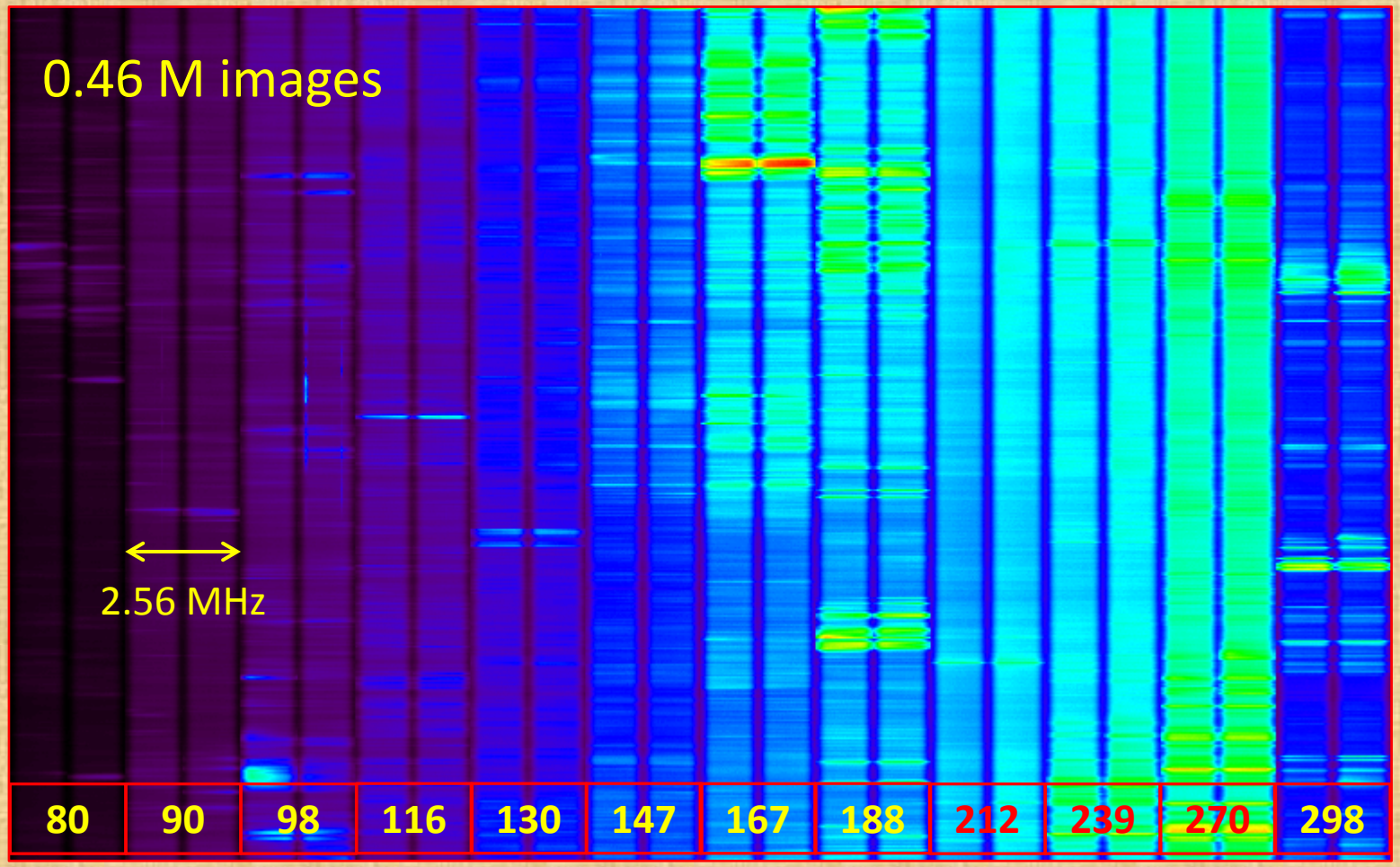
Sampling in tl





Snapshot uv coverage at 285 MHz

Sample MWA Dynamic Spectrum

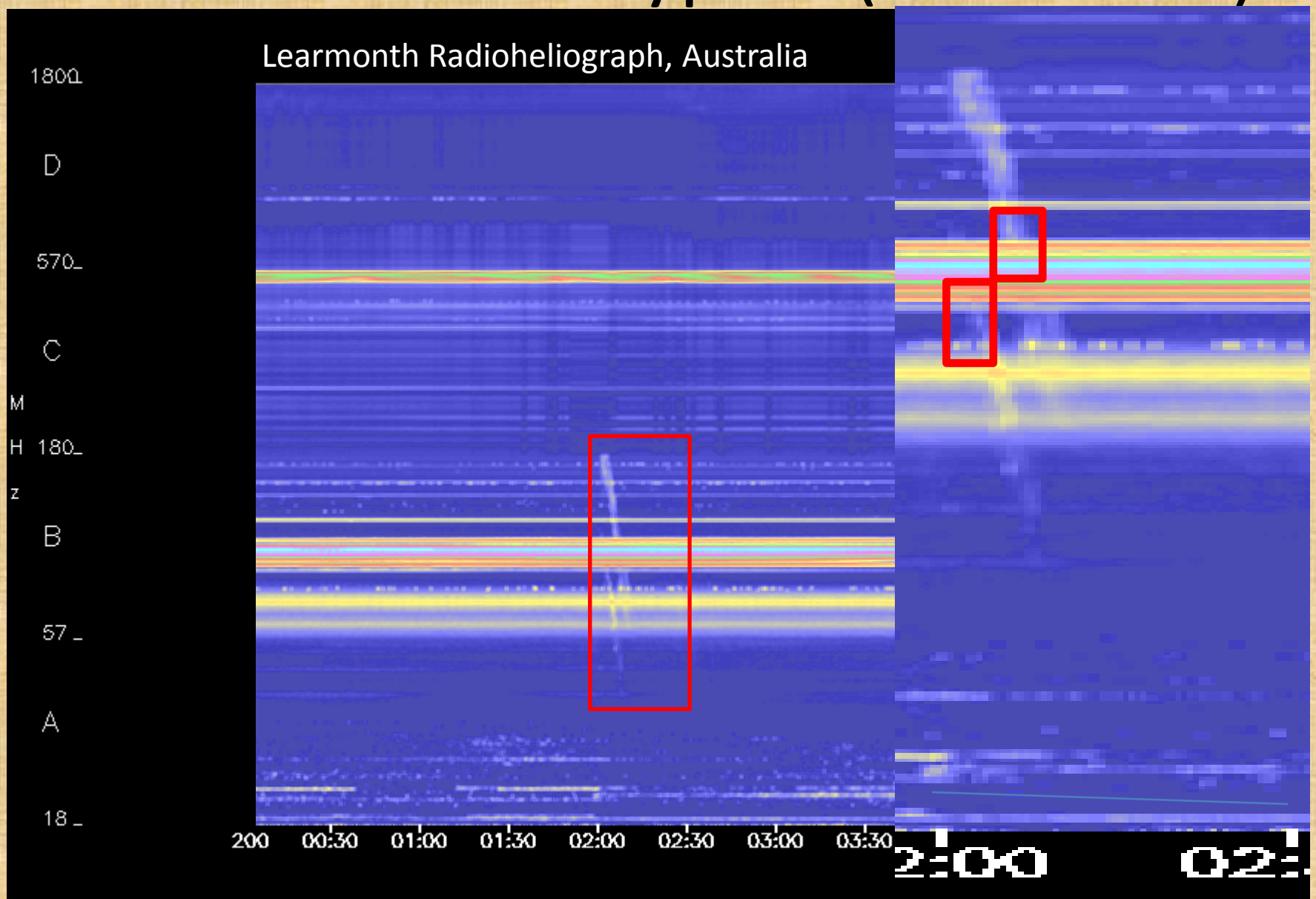


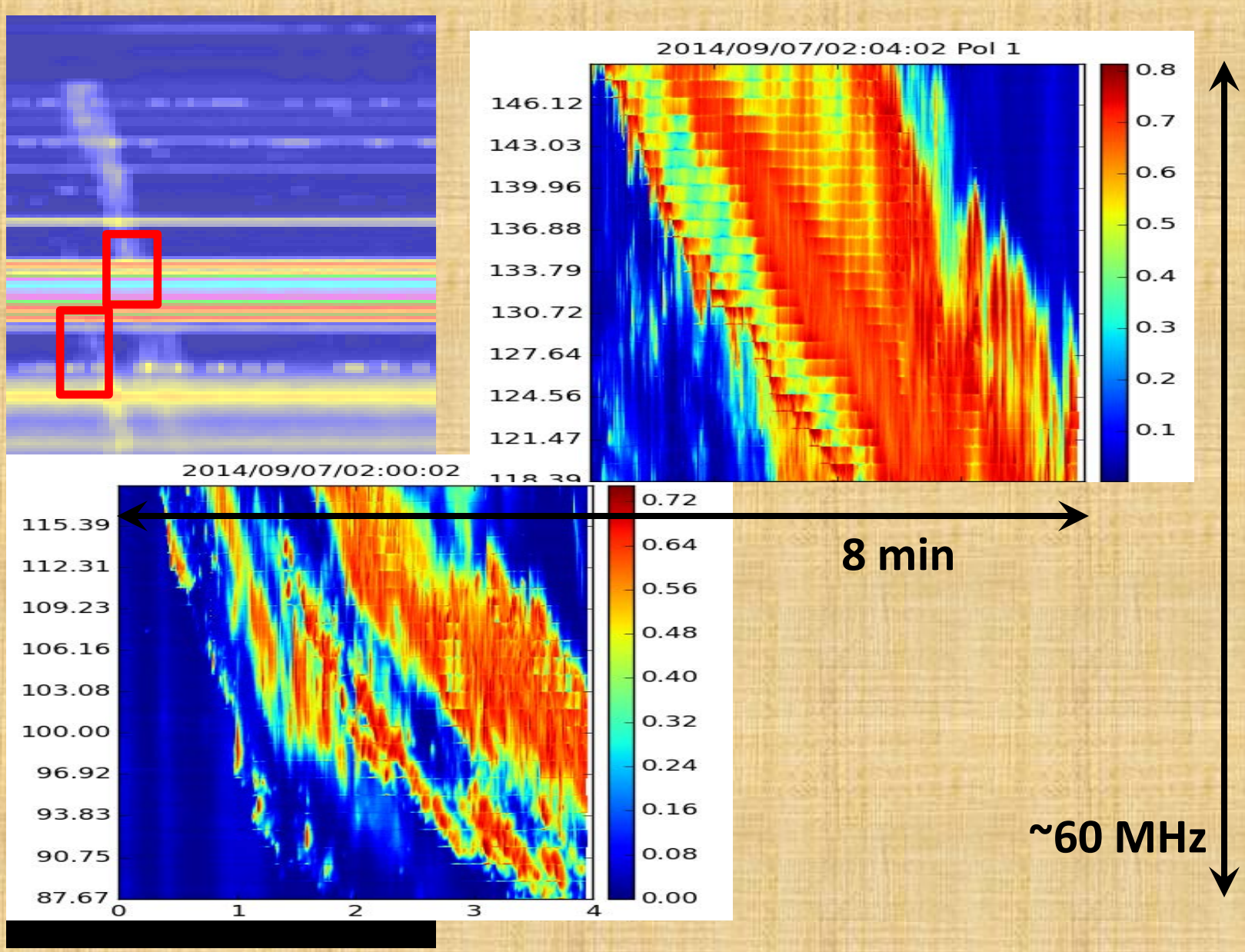
Time (5 min)

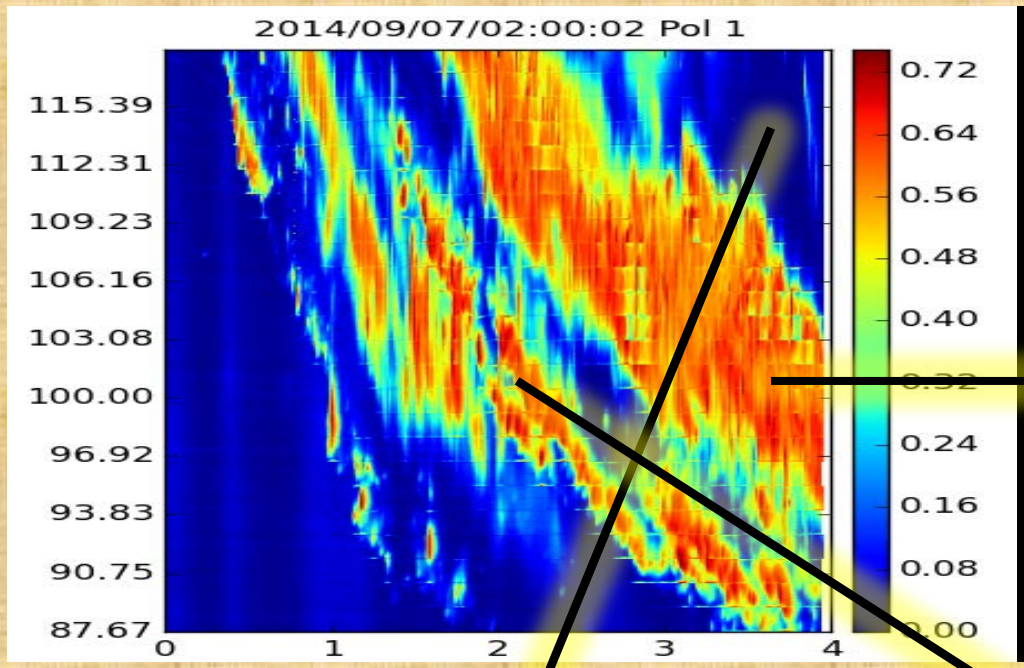
Frequency

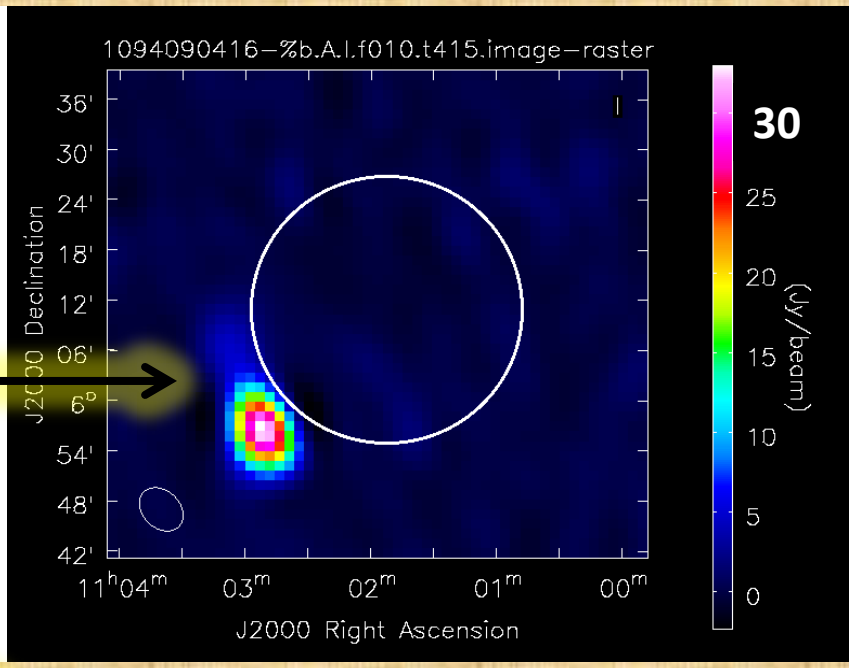
(12 log-spaced groups of 2.56 MHz spanning 80 – 300 MHz)

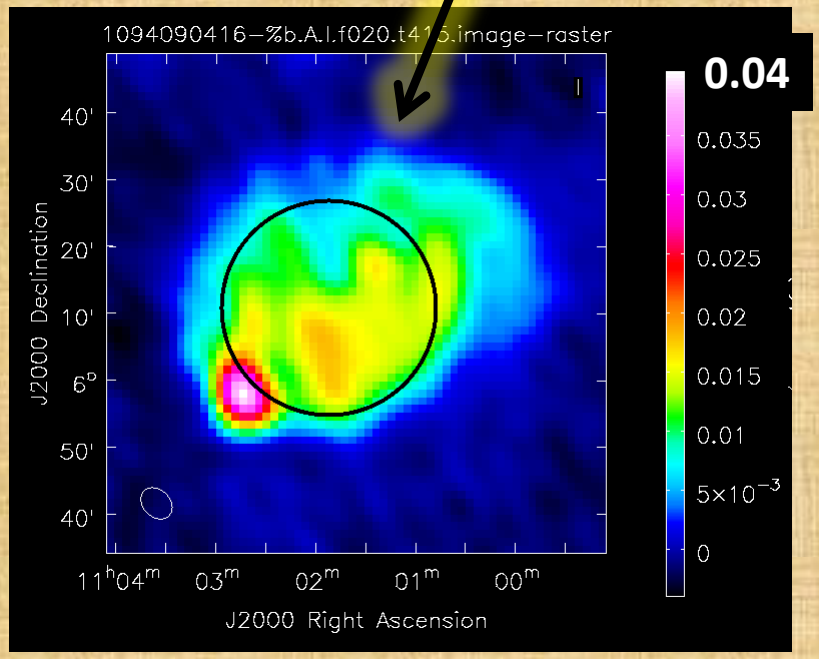
The first MWA type II (20140907)

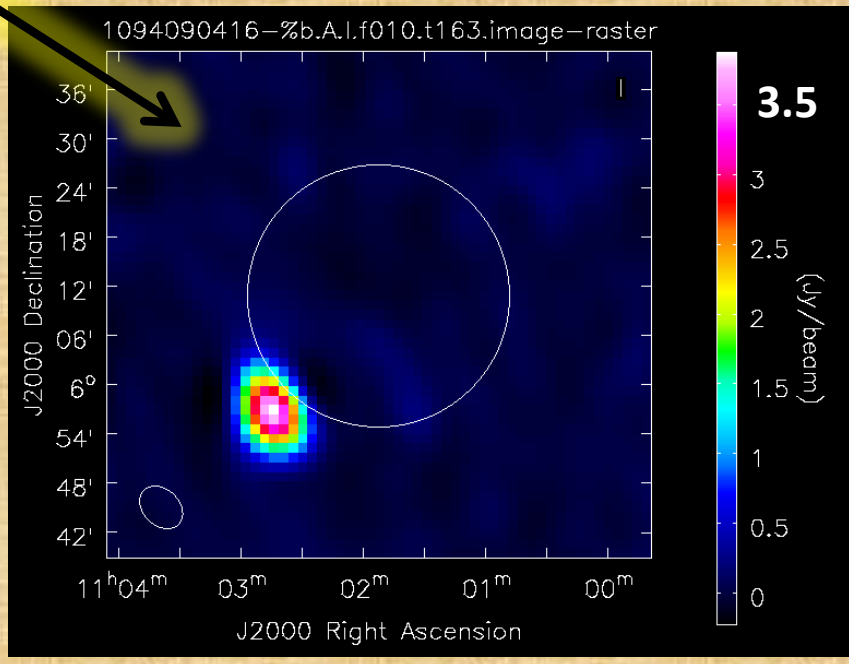



2014/09/07/02:04:02 Pol 1
146.12
143.03
139.96
136.88
133.79
130.72
127.64
124.56
121.47
0.8
0.7
0.6
0.5
0.4
0.3
0.2
0.1
2014/09/07/02:00:02
115.39
112.31
109.23
106.16
103.08
100.00
96.92
93.83
90.75
87.67
0
1
2
3
4
0.72
0.64
0.56
0.48
0.40
0.32
0.24
0.16
0.08
0.00
8 min
~60 MHz

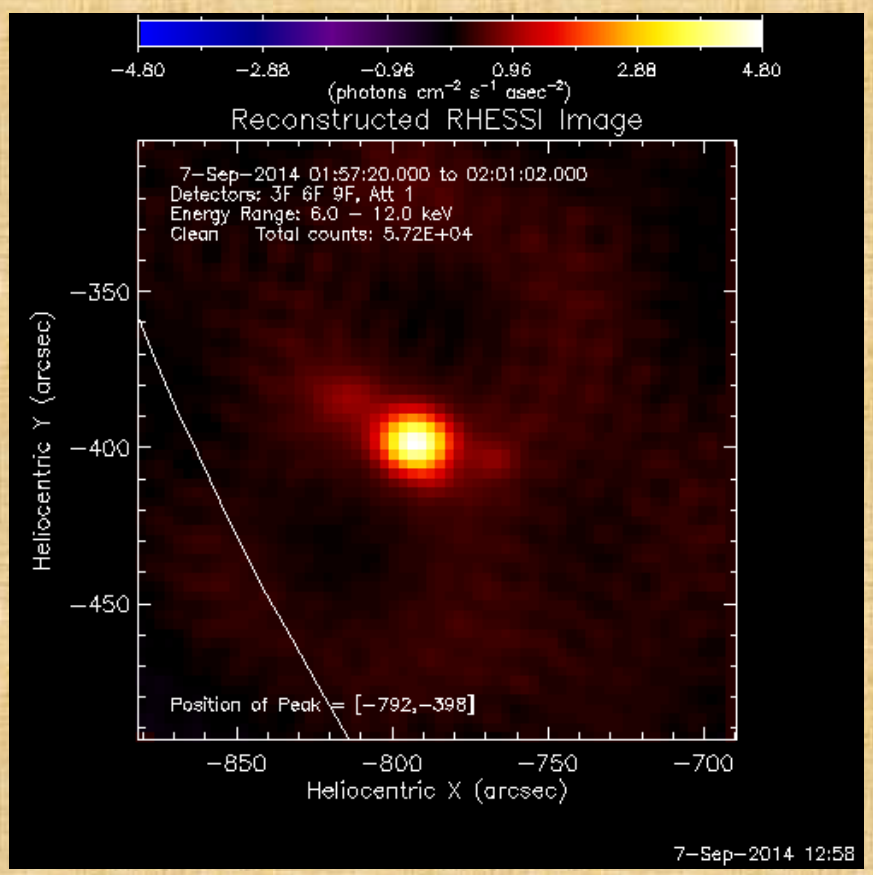

2014/09/07/02:00:02 Pol 1
115.39
112.31
109.23
106.16
103.08
100.00
96.92
93.83
90.75
87.67
0
1
2
3
4
0.72
0.64
0.56
0.48
0.40
0.24
0.16
0.08

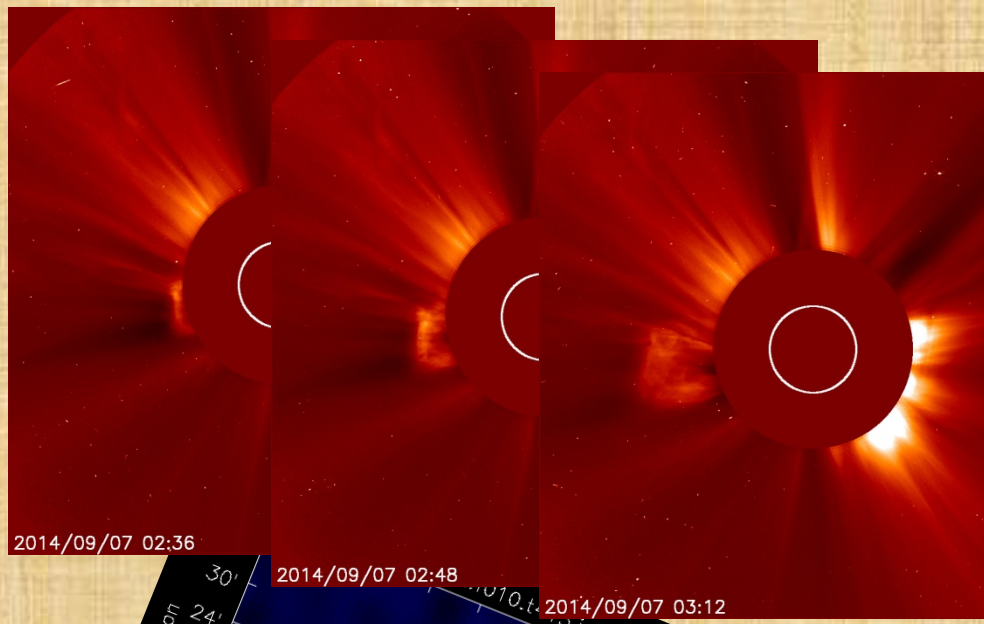

1094090416–%b.A.I.f010.t415.image–raster
36'
30'
24'
18'
12'
06'
6°
54'
48'
42'
J2000 Declination
11h04m
03m
02m
01m
00m
J2000 Right Ascension
30
25
20
15
10
5
0
(Jy/beam)

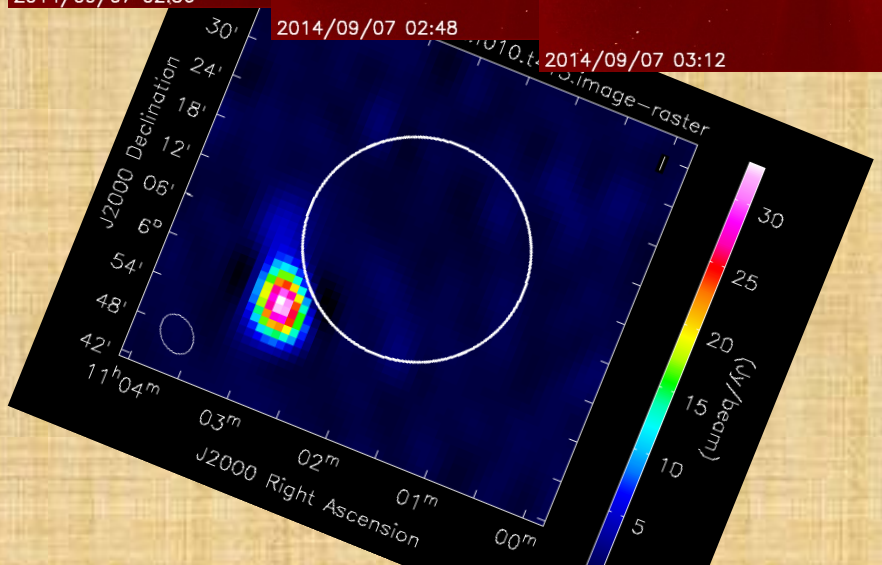

1094090416–%b.A.I.f020.t415.image–raster
40'
30'
20'
10'
6°
50'
40'
J2000 Declination
11h04m
03m
02m
01m
00m
J2000 Right Ascension
0.04
0.035
0.03
0.025
0.02
0.015
0.01
5×10−3
0

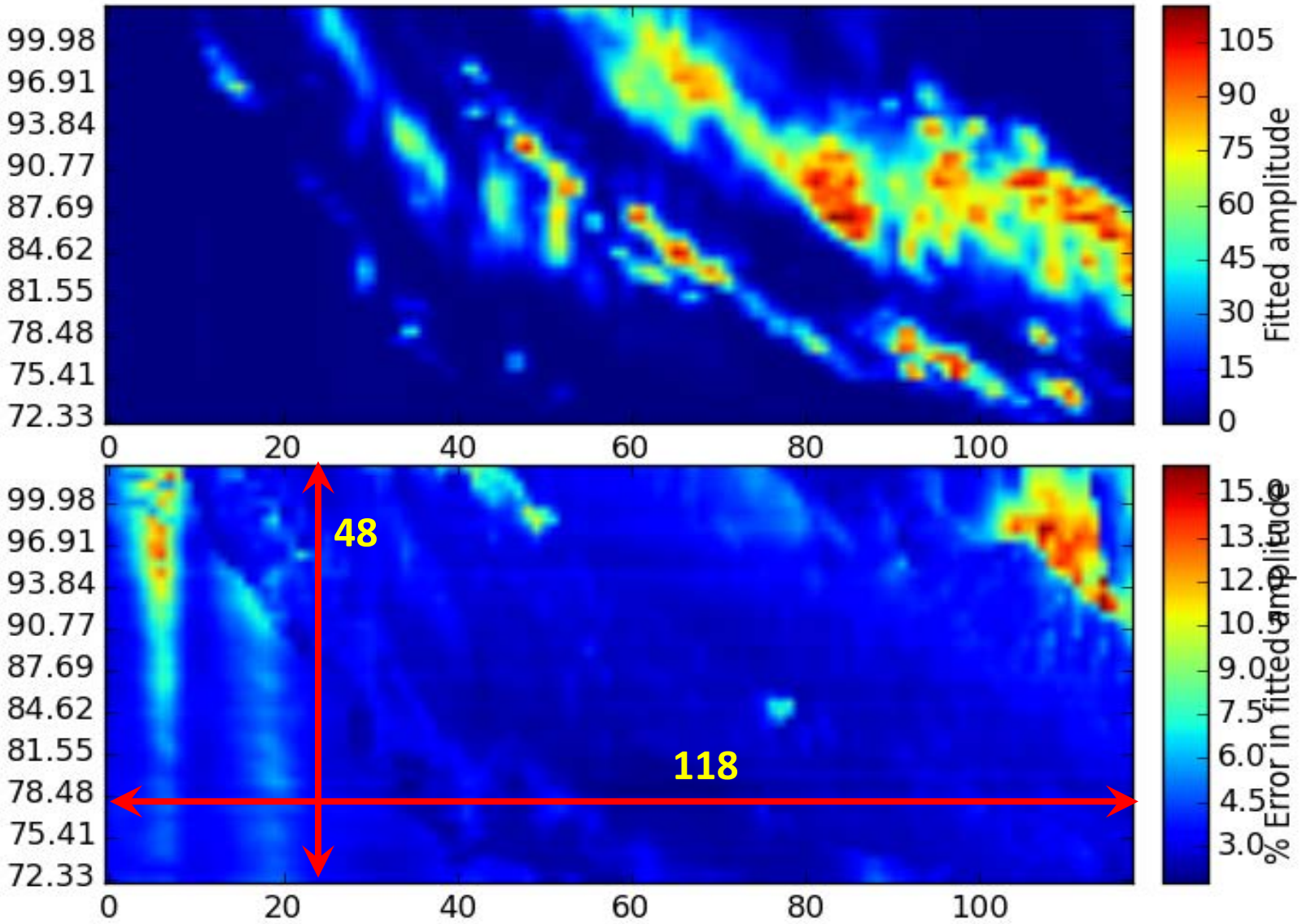

1094090416–%b.A.I.f010.t163.image–raster
36'
30'
24'
18'
12'
06'
6°
54'
48'
42'
J2000 Declination
11h04m
03m
02m
01m
00m
J2000 Right Ascension
3.5
3
2.5
2
1.5
1
0.5
0
(Jy/beam)

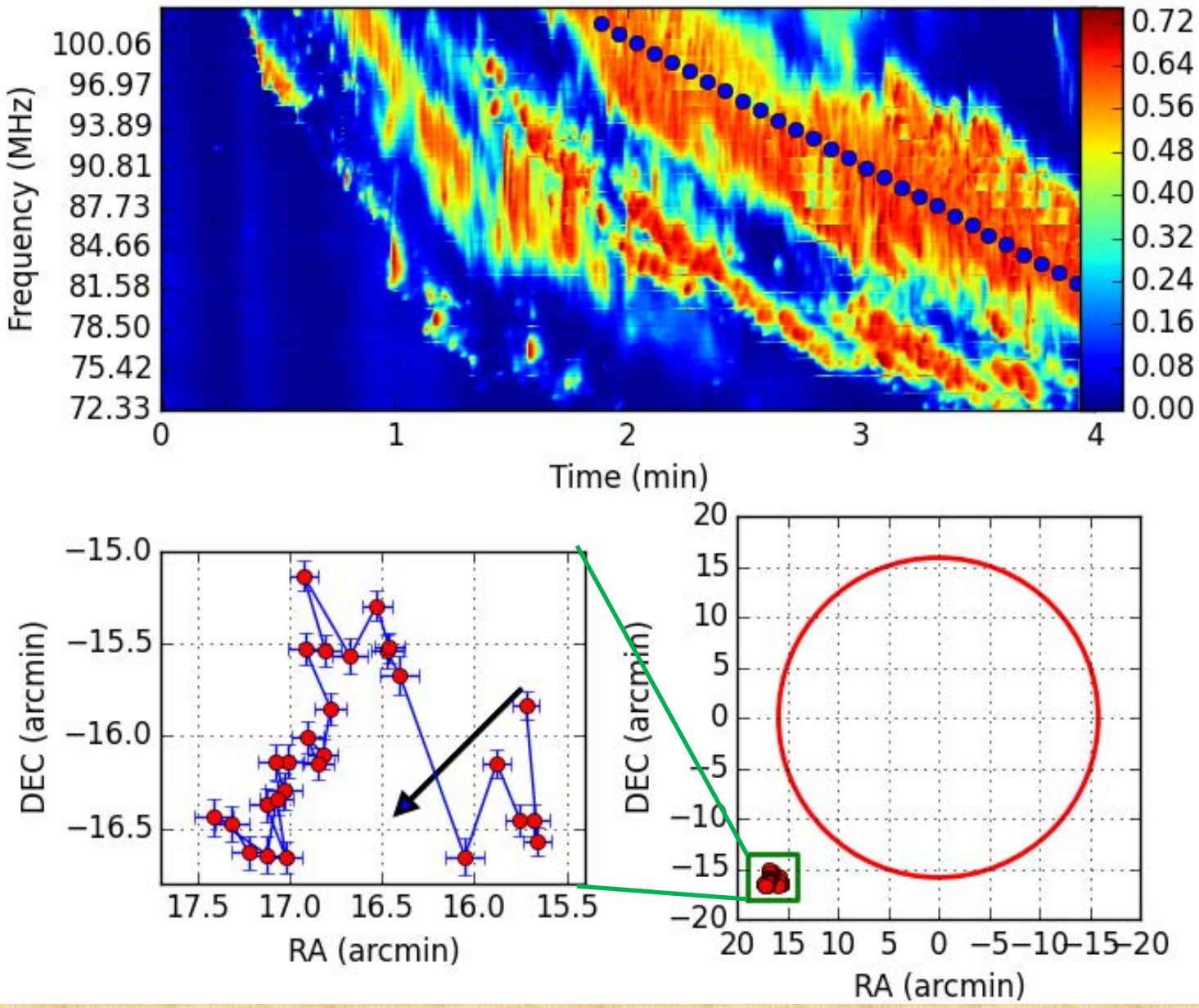
RHESSI X-ray source: Visible disk near South-East limb ➔ plausible source of CME seen by LASCO



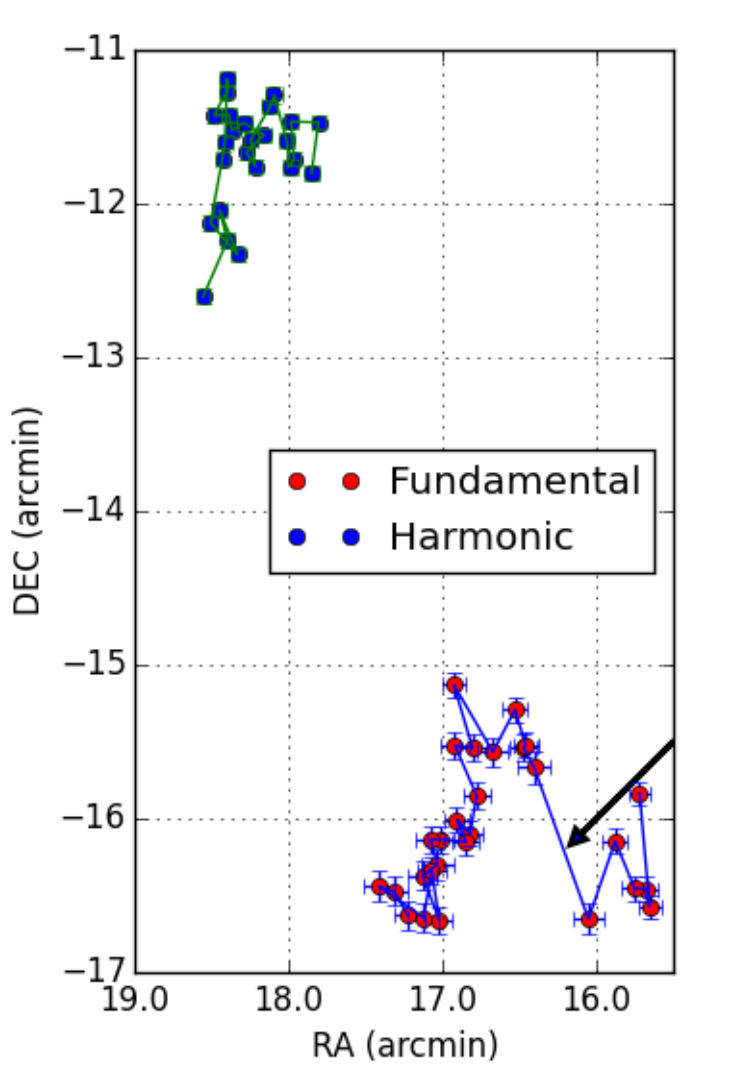





99.98
96.91
93.84
90.77
87.69
84.62
81.55
78.48
75.41
72.33
0
20
40
60
80
100
105
90
75
60
45
30
15
0
Fitted amplitude
48
118
% Error in fitted amplitude

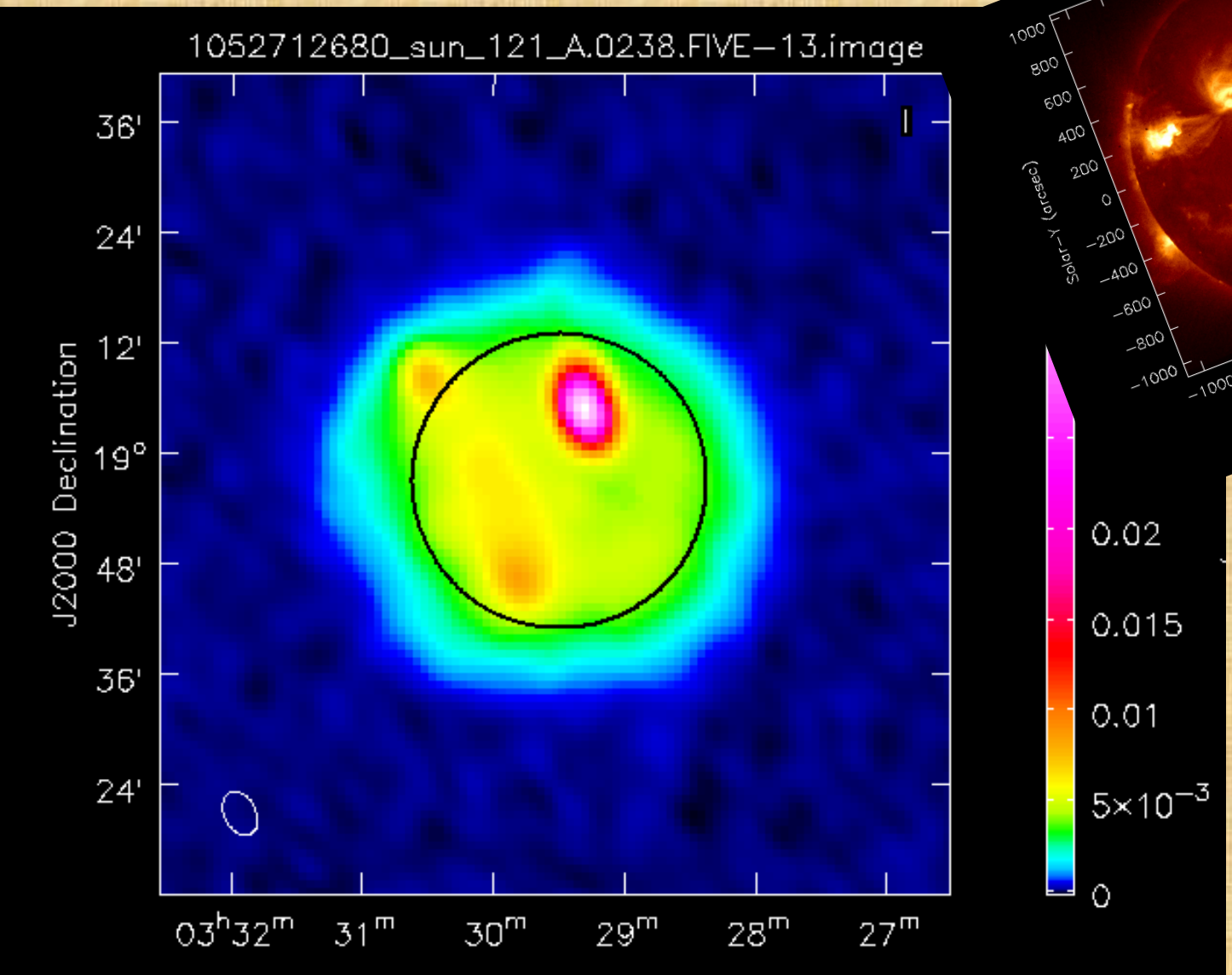

Frequency (MHz)
100.06
96.97
93.89
90.81
87.73
84.66
81.58
78.50
75.42
72.33
0
1
2
3
4
Time (min)
0.72
0.64
0.56
0.48
0.40
0.32
0.24
0.16
0.08
0.00
DEC (arcmin)
−15.0
−15.5
−16.0
−16.5
17.5
17.0
16.5
16.0
15.5
RA (arcmin)
DEC (arcmin)
20
15
10
5
0
−5
−10
−15
−20
20 15 10 5 0 −5 −10 −15 −20
RA (arcmin)

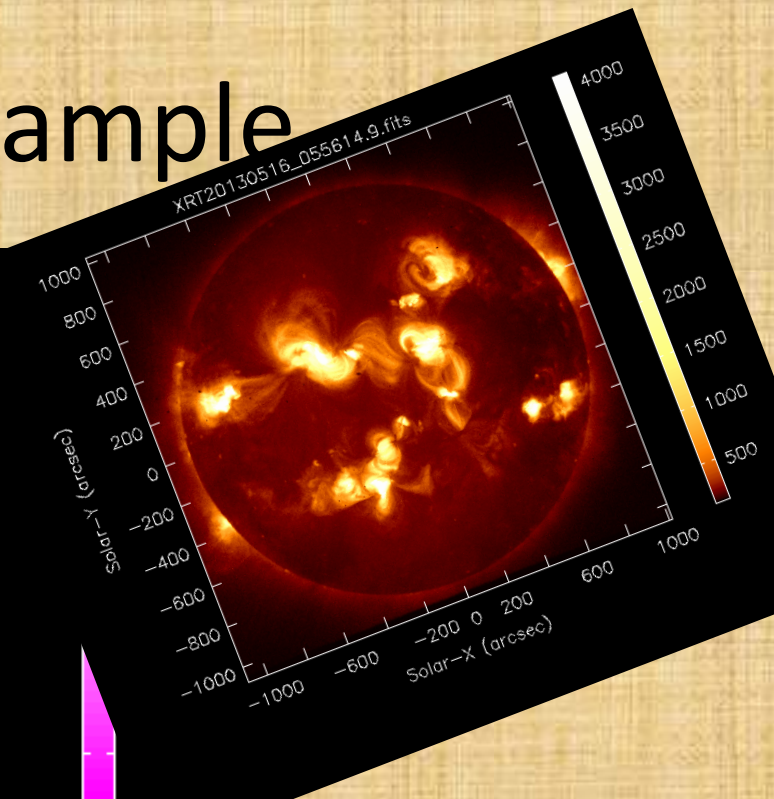
Key points



- The type II source is a compact, a slightly resolved source (1.2-1.4 x the resolution)
- Height ~1.4 R_{Sun}
- Fundamental and Harmonic emission do not appear to be coincident
- Locations of F emission show a larger scatter than H

An Imaging Example





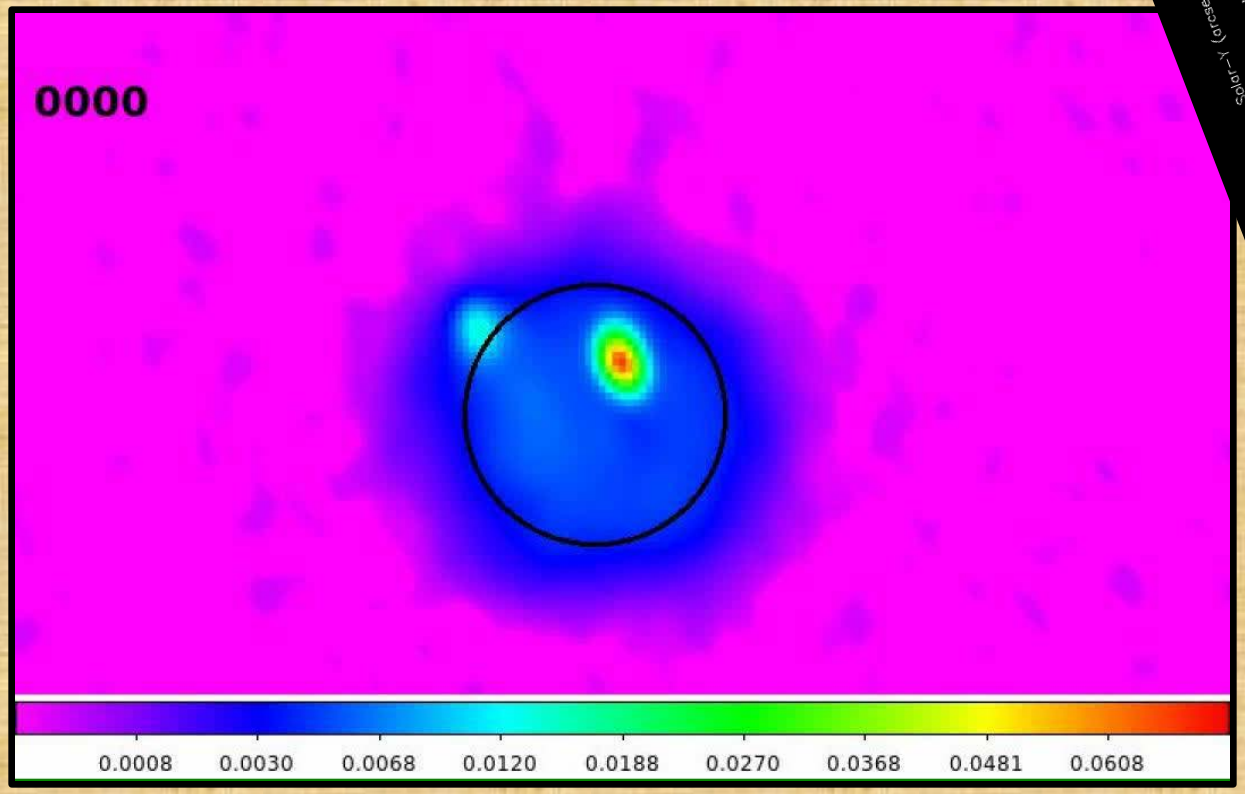
16 May, 2013
04:15:02 UT

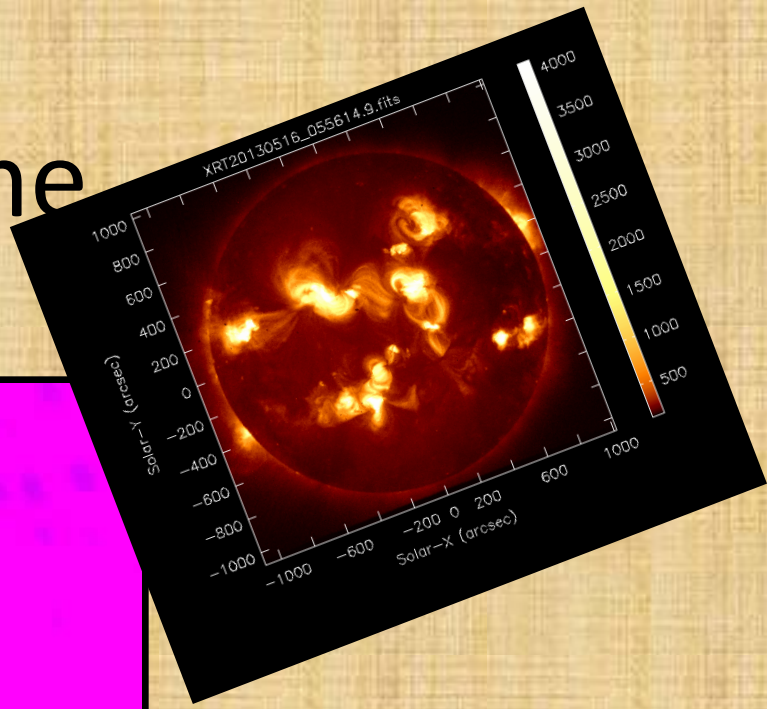
ν_0=153.905 MHz
$\Delta\nu$=640 kHz

Δt=1 second

Imaging Dynamic Range ~1400

Movie Time





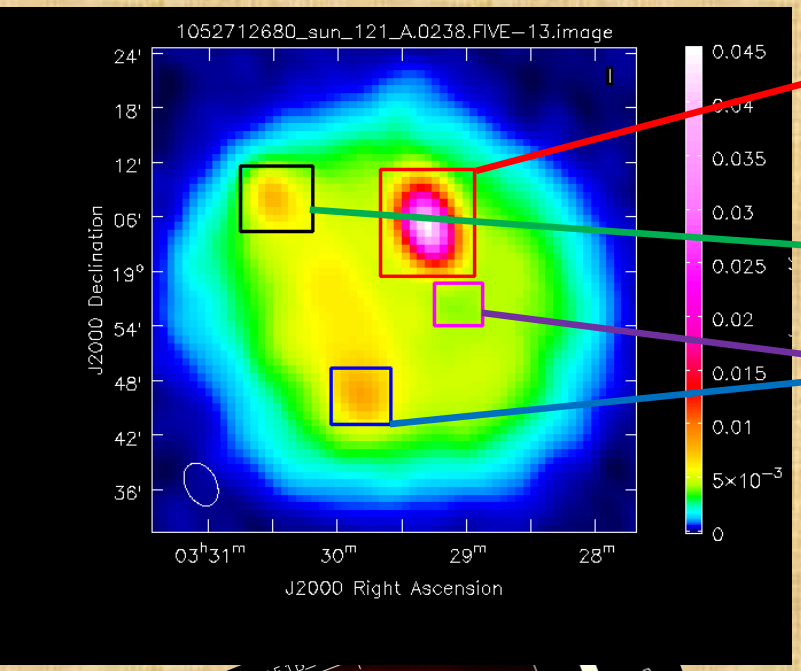
16 May, 2013
04:11:04 – 04:16:00 UT

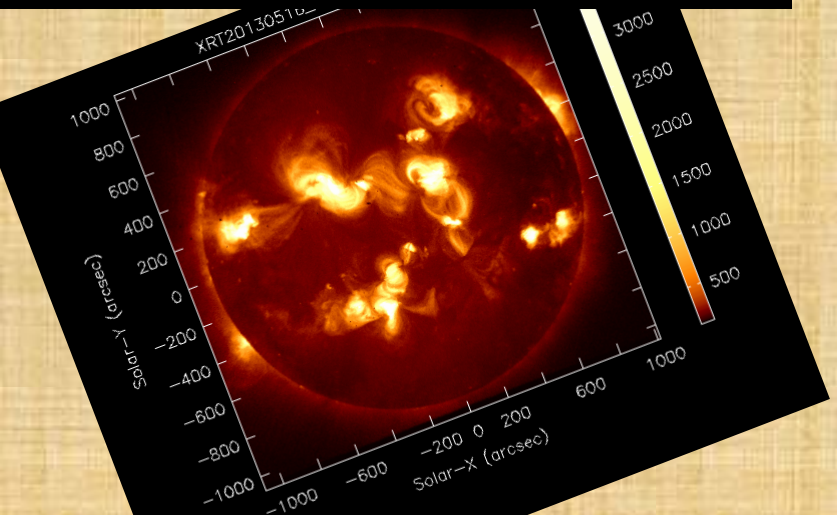
ν_0=153.905 MHz
$\Delta\nu$=640 kHz

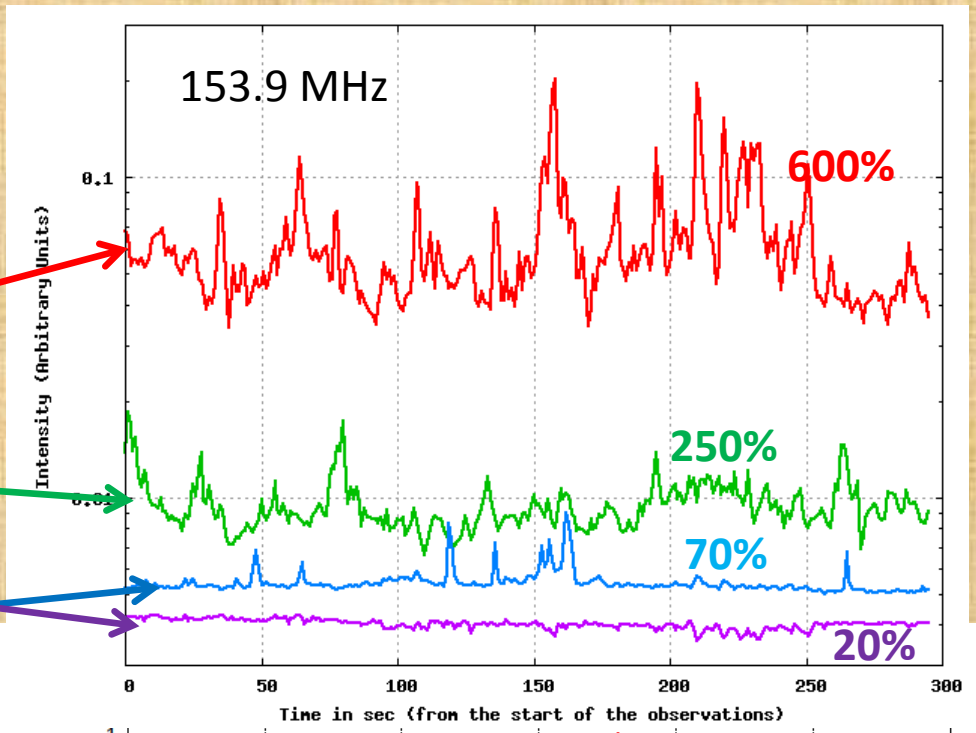
Δt=1 second

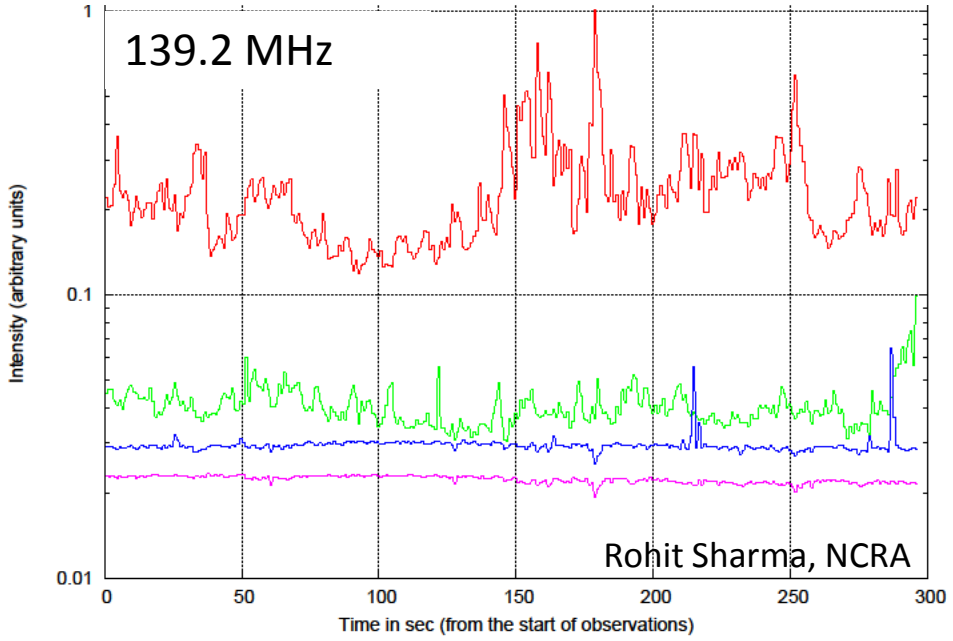
Imaging Dynamic Range
~1400

Spatial Variability

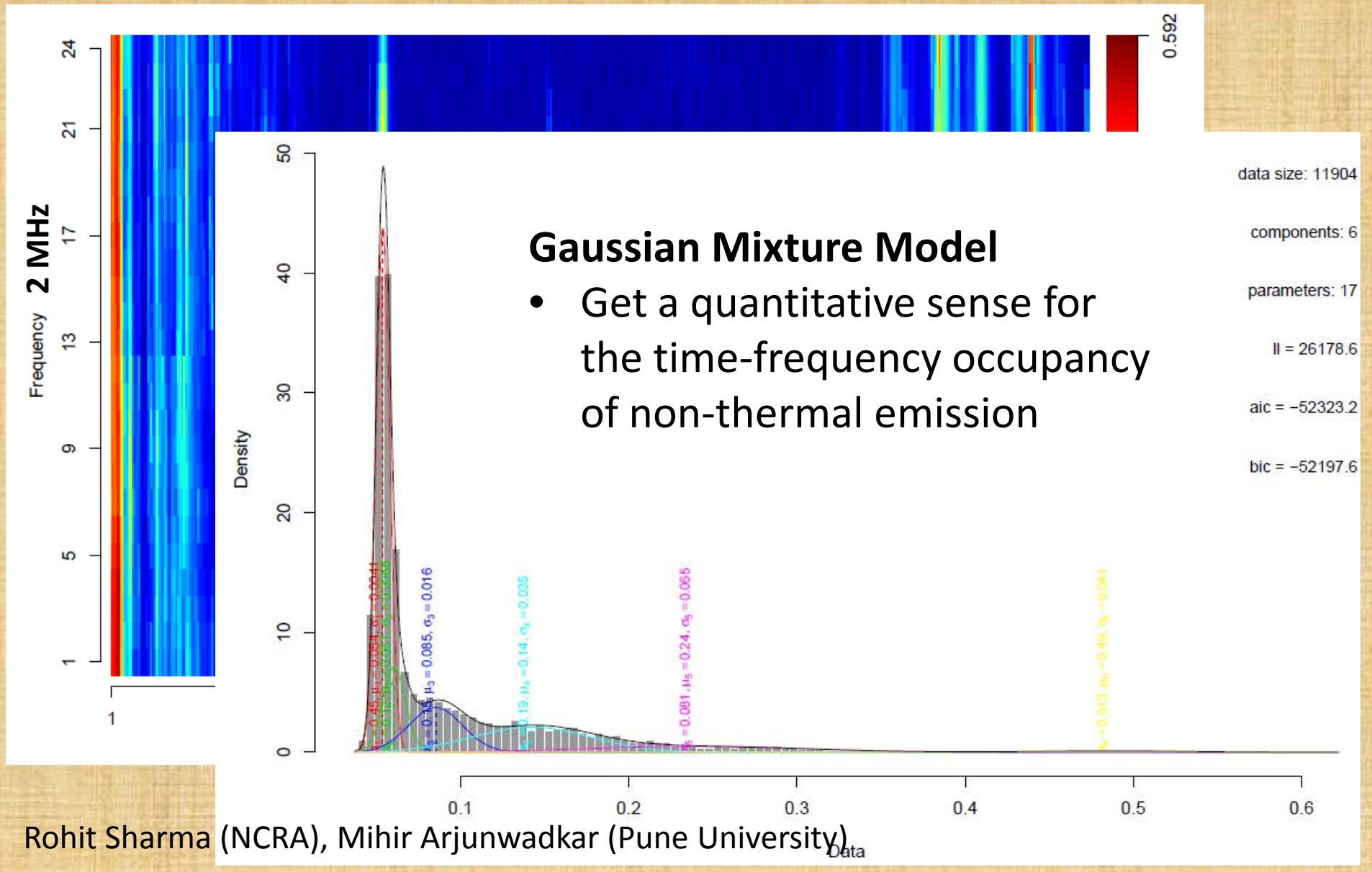








Studying weak non-thermal emission

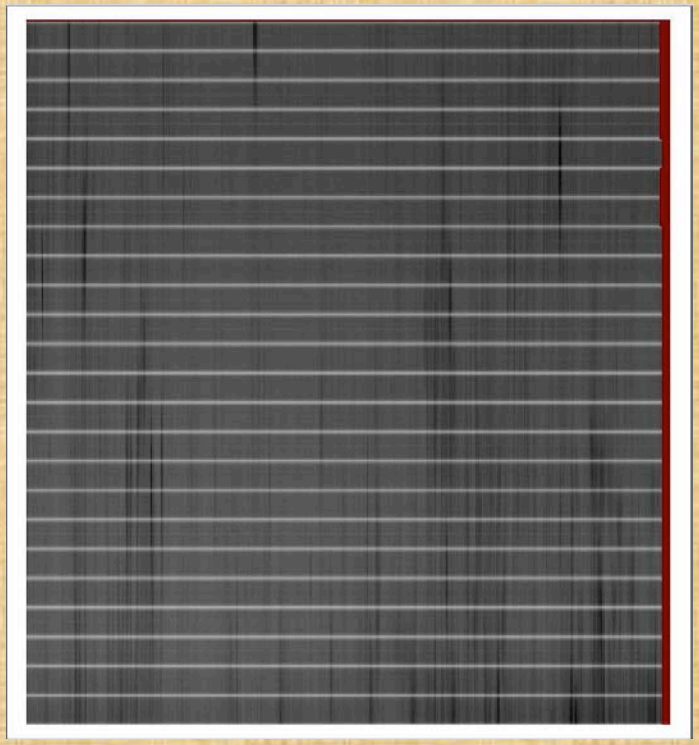


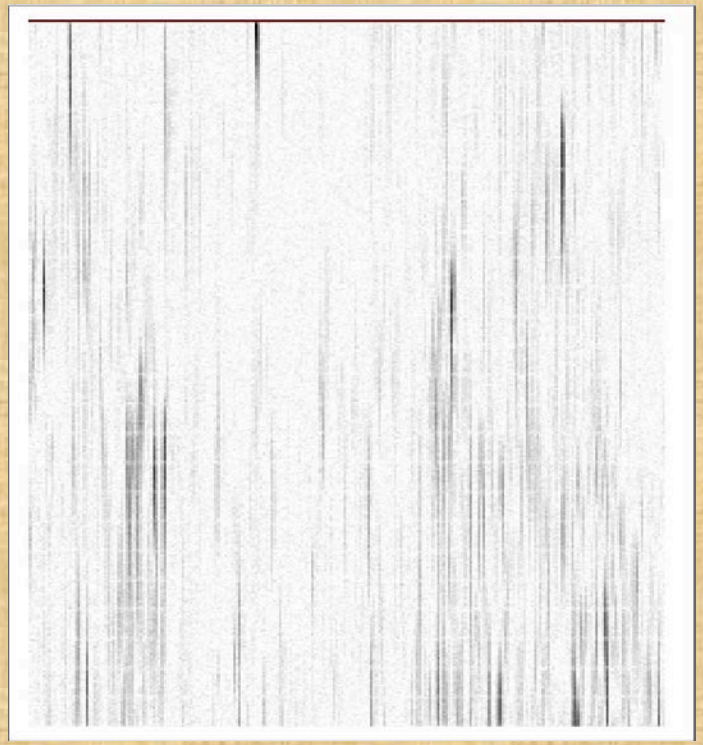
Gaussian Mixture Model

- Get a quantitative sense for the time-frequency occupancy of non-thermal emission

Rohit Sharma (NCRA), Mihir Arjunwadkar (Pune University)

Automated characterization of non-thermal emission features



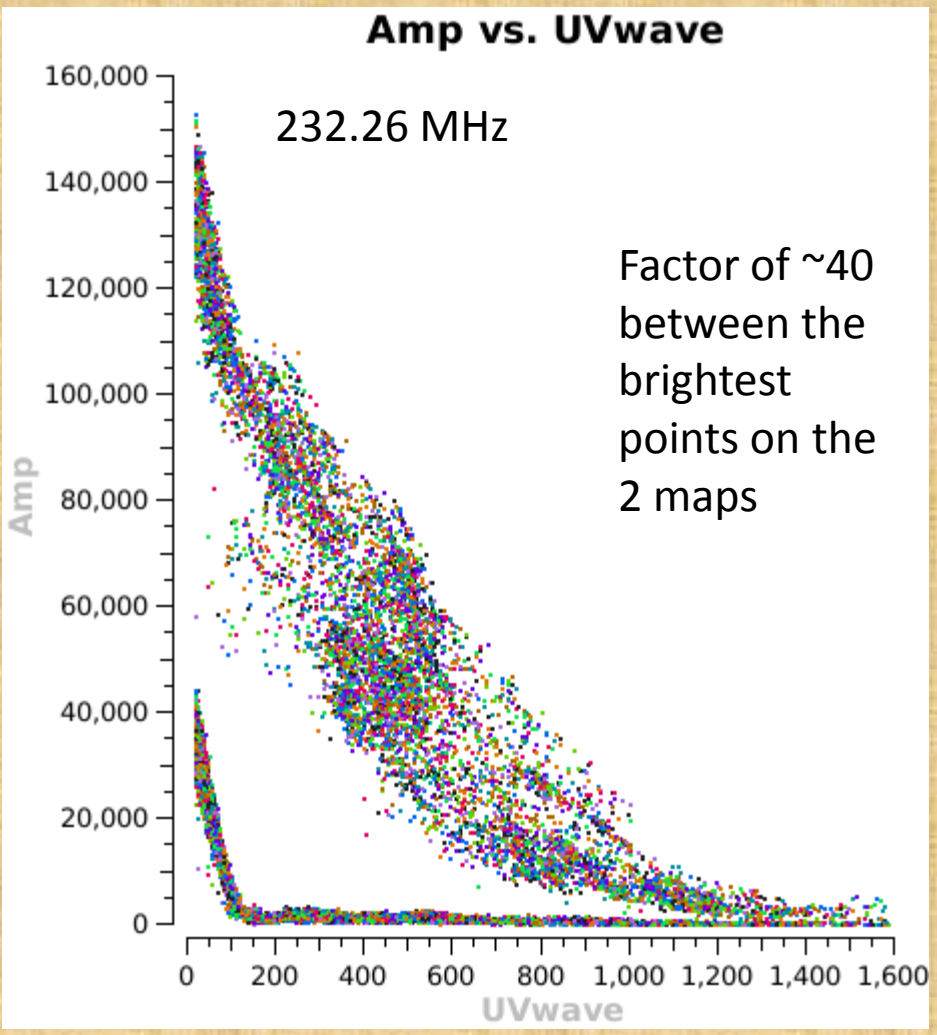


- Characterizing the ‘shapes’ and profiles of non-thermal emissions in the dynamic spectra
- Wavelet decomposition approach seems promising

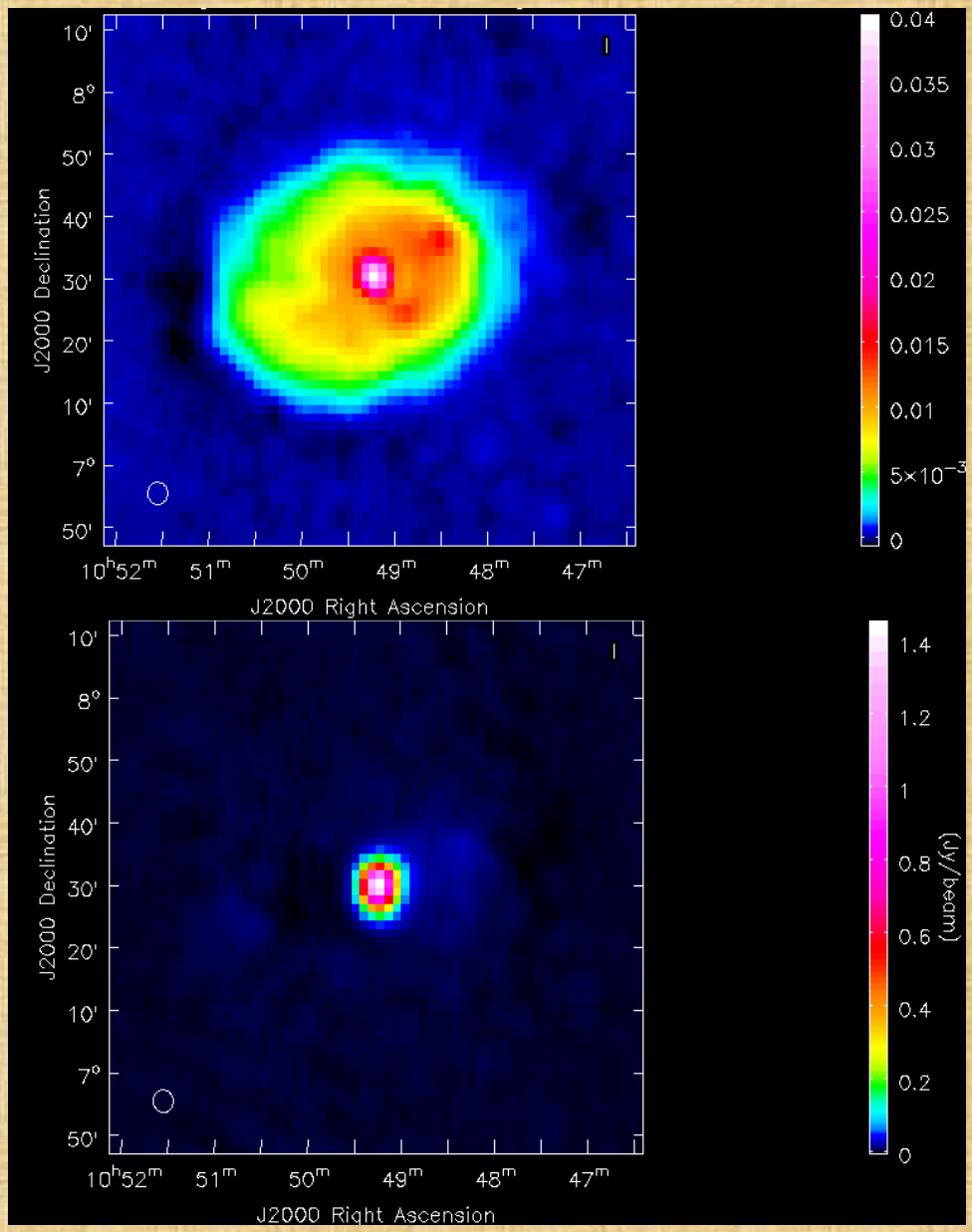
Summary

- Radio observations offer views complementary to those from other wavebands and offer some unique diagnostics.
- With the advent of new generation instruments, we can expect radio data to play a larger role in solar physics.
- Key solar science enabling capability - High fidelity wideband spectroscopic imaging capability with high time and frequency resolution, and sufficient angular resolution
- Of the low frequency instruments available, the MWA is by far the best suited for solar science.
- Moving from a science commissioning/ 'understanding the data' phase to science phase
- Stay tuned…

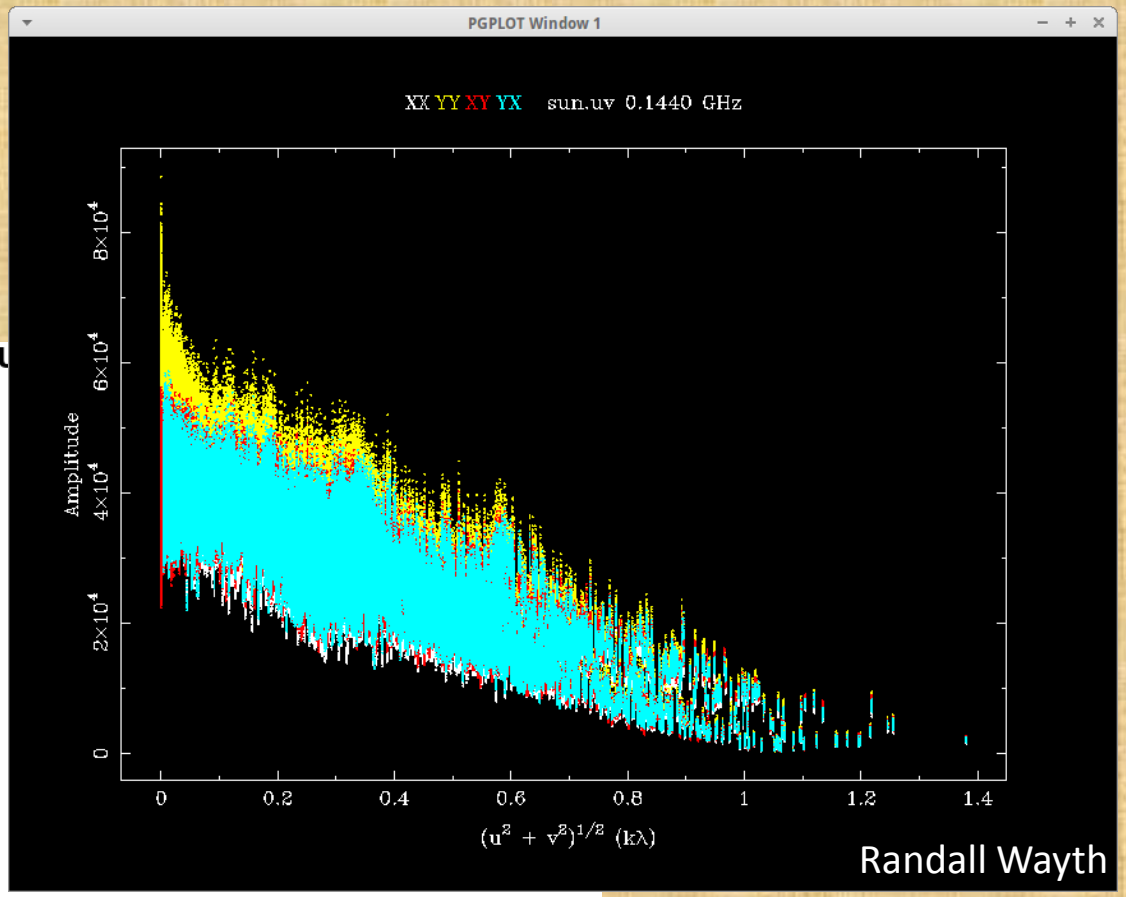
Quiet vs Active Sun

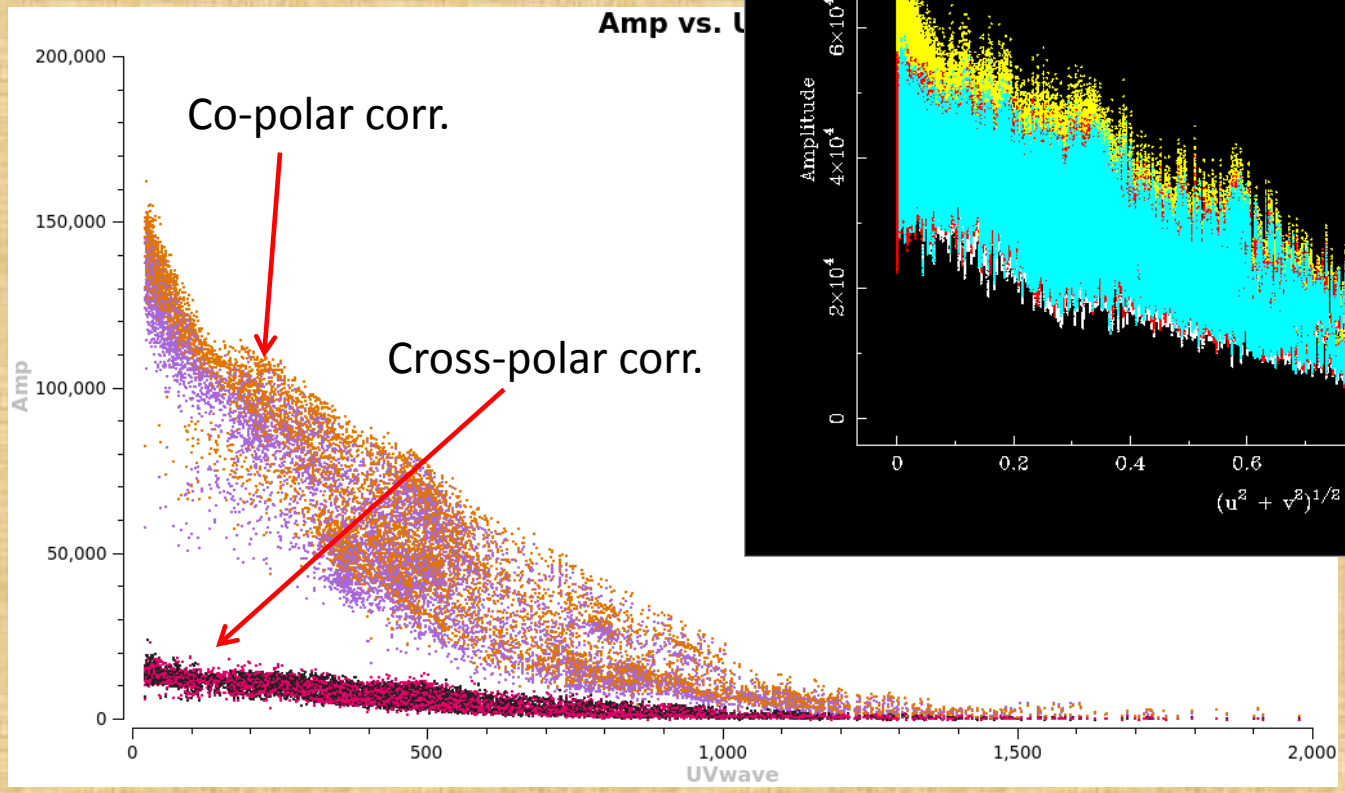


Factor of ~40 between the brightest points on the 2 maps



Variations in polarization signatures

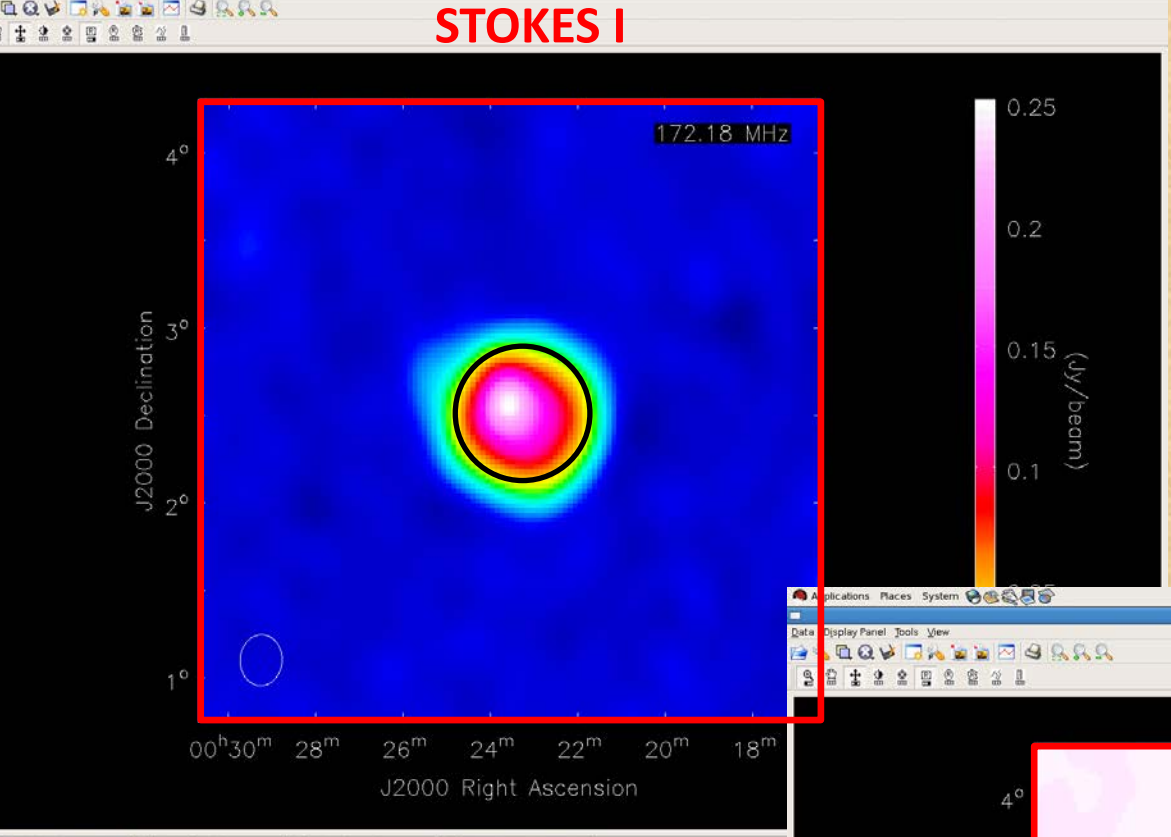


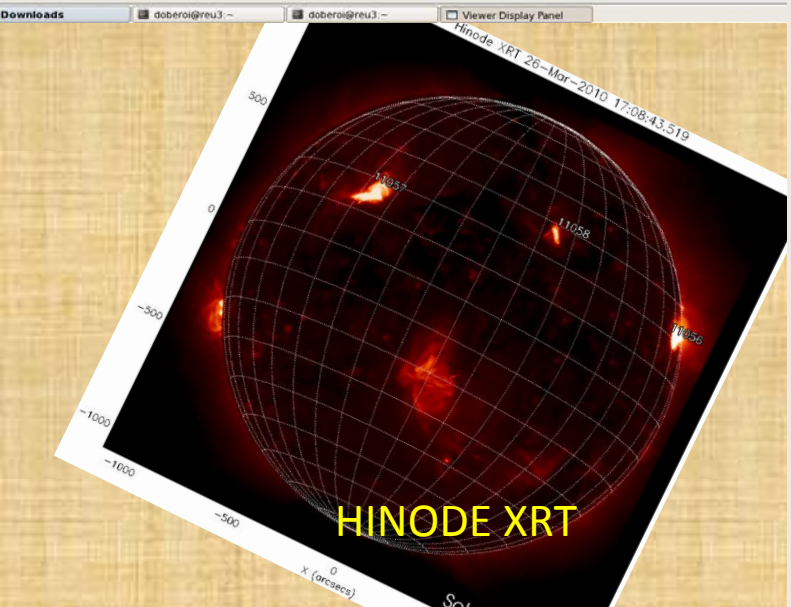


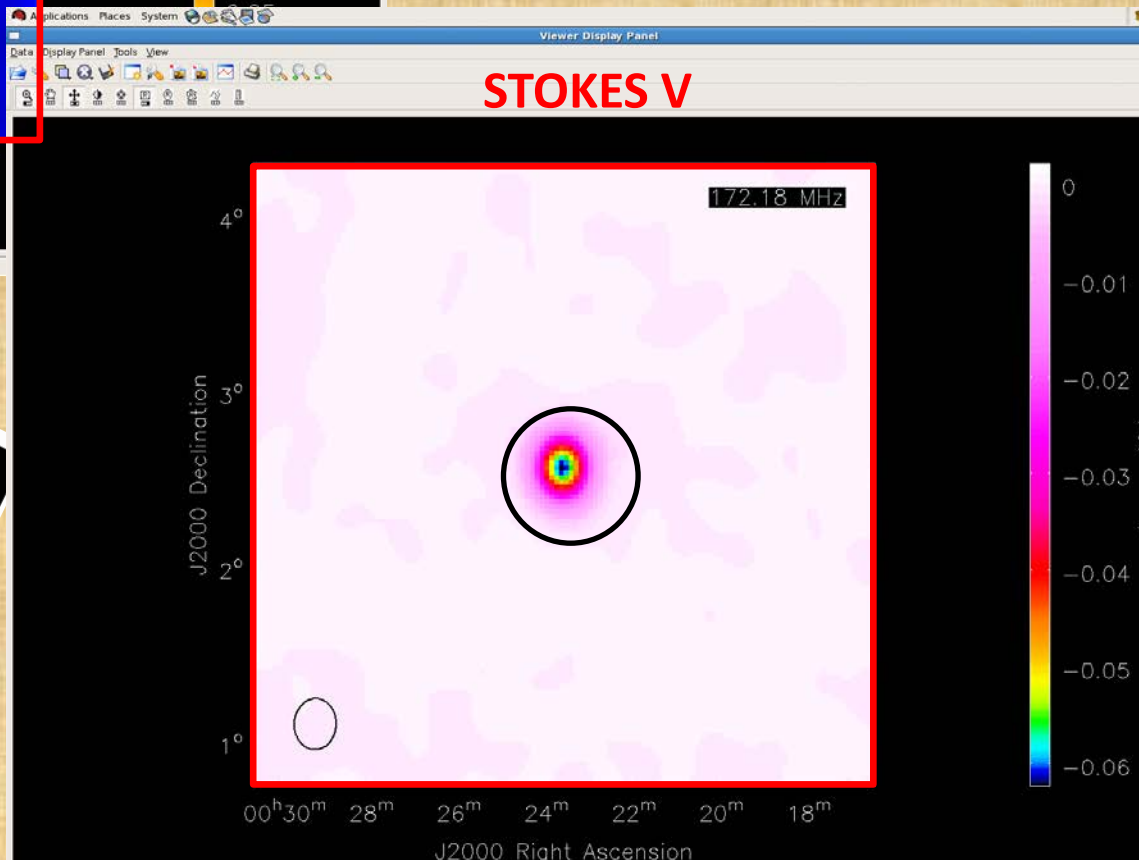
Detection of Stokes V from an active region

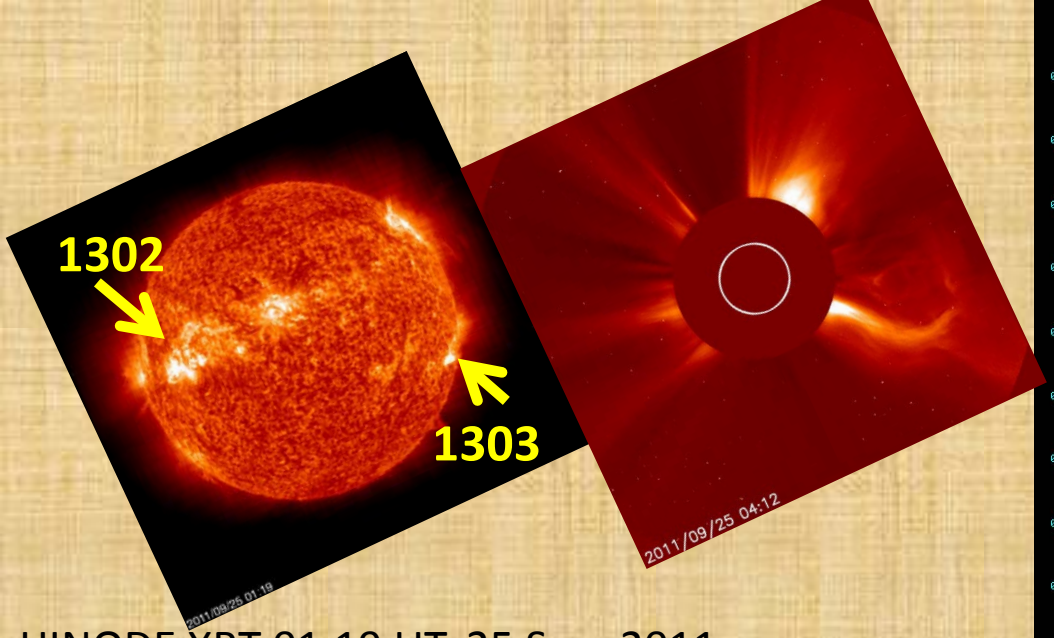
Each image corresponds to 1 s and 40 kHz integration

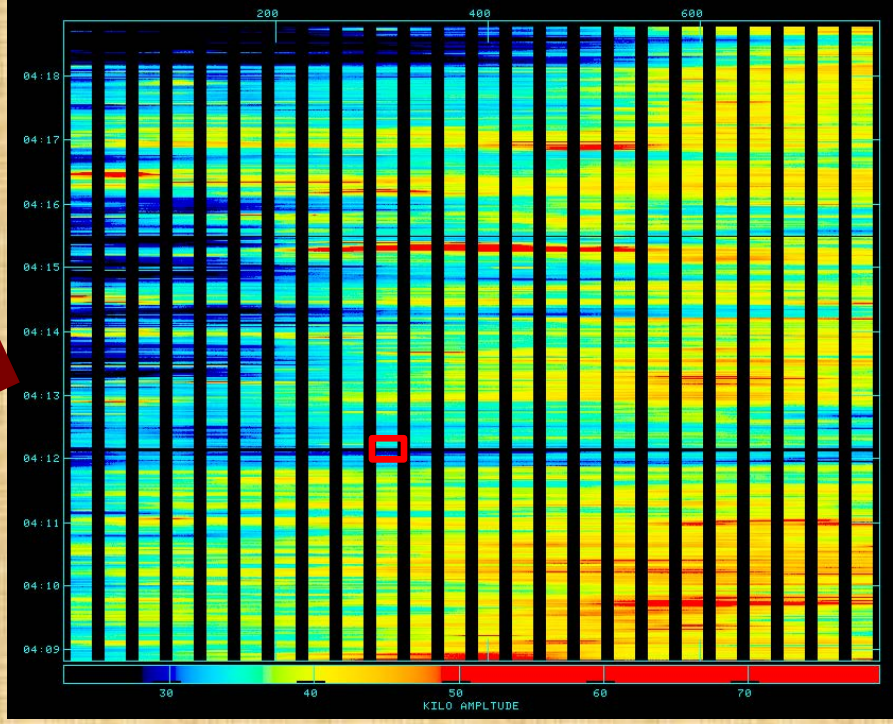
Frames 1.28 MHz apart, span ~170-200 MHz for the same time slice







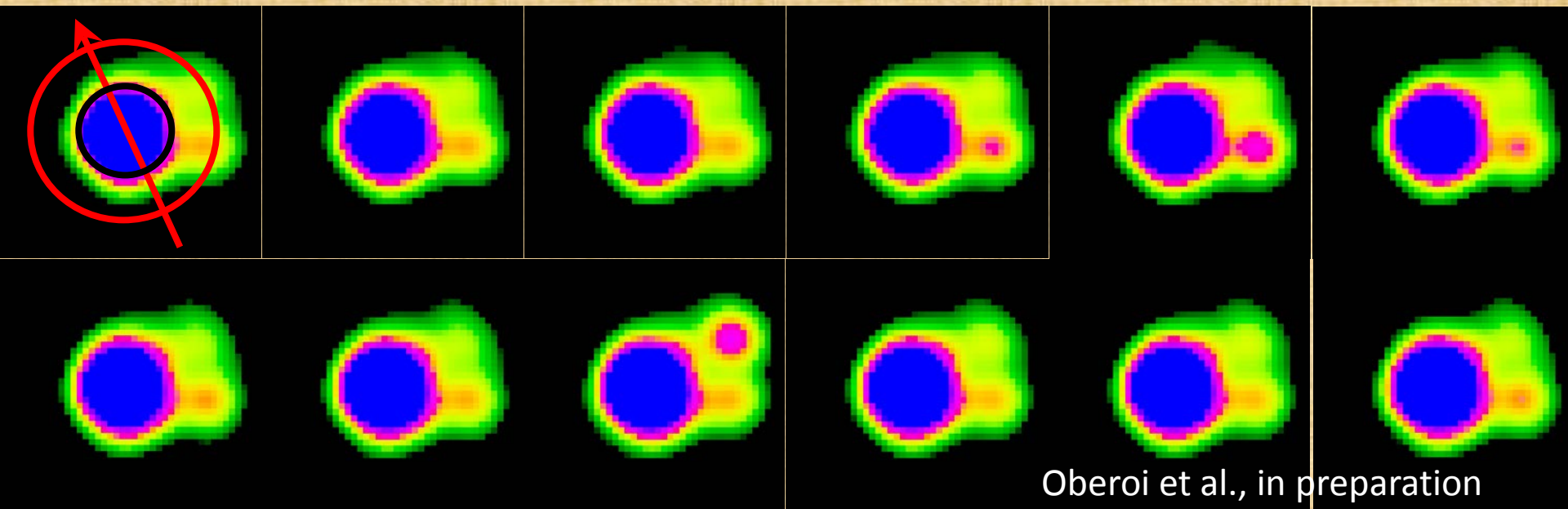




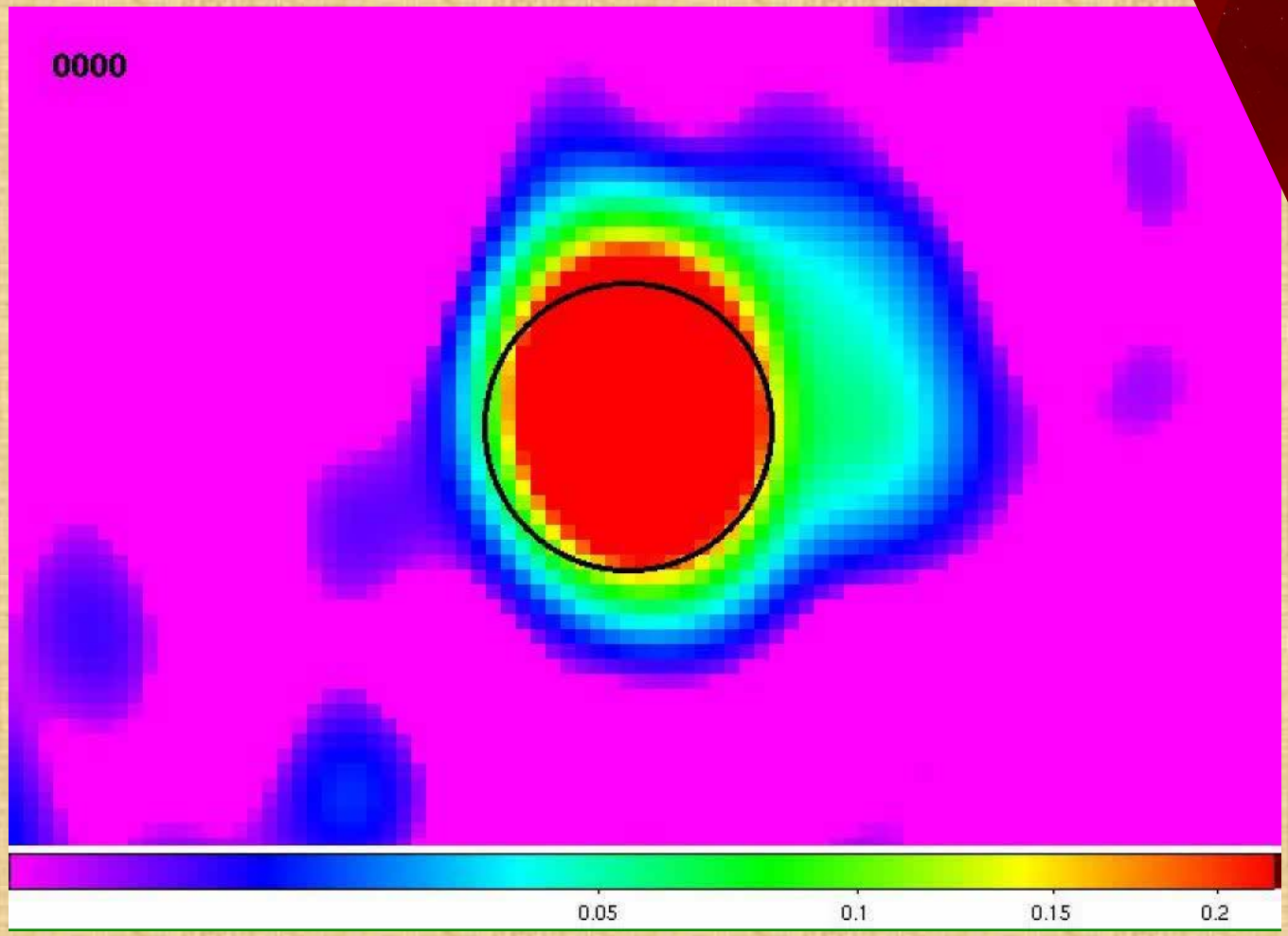
HINODE XRT 01:19 UT, 25 Sep. 2011

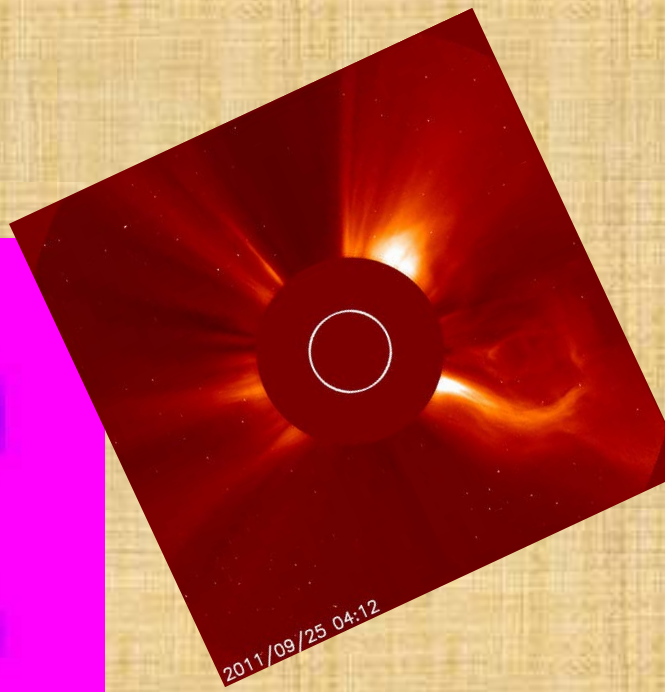
SOHO/LASCO C2 at 04:12 UT (19 s integration)

32T 152.3 MHz, 1s, 80 kHz, θ_0=13.3', log scale, DR ~1100, images are 1 s apart



Oberoi et al., in preparation



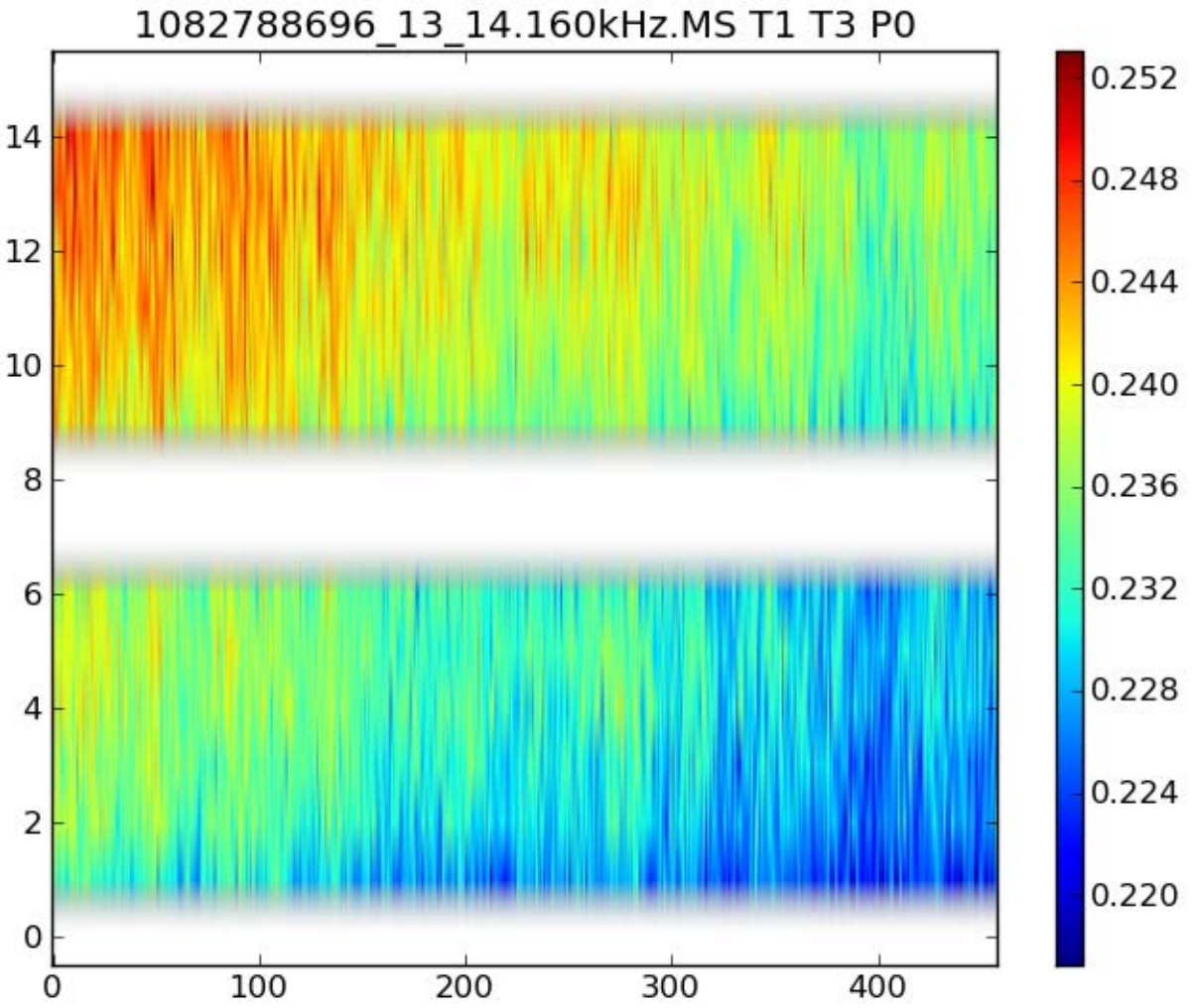


25 Sep, 2011
04:08:50 – 04:18:47 UT

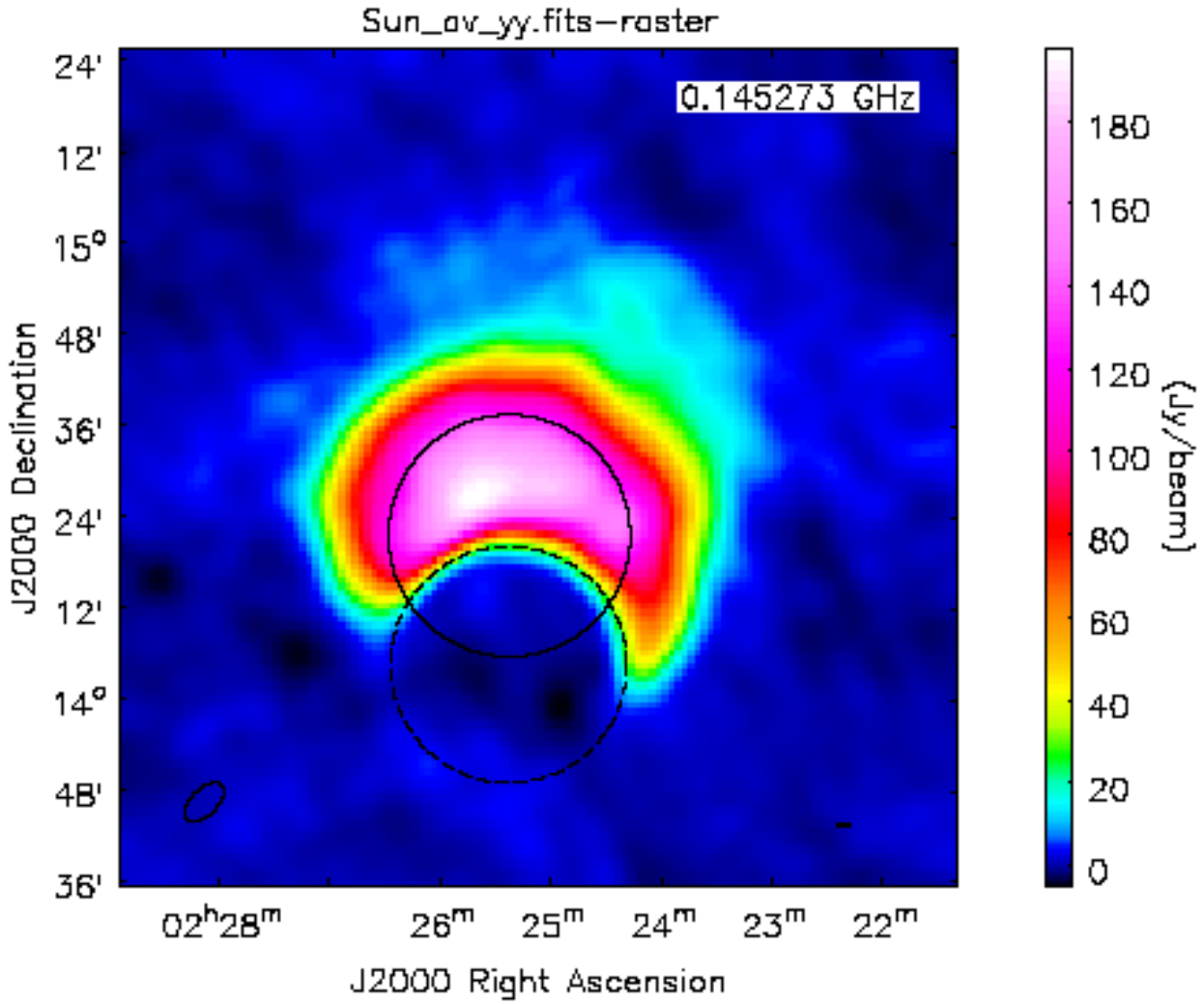
ν_0=152.3 MHz
$\Delta\nu$=80 kHz

Δt=1 second

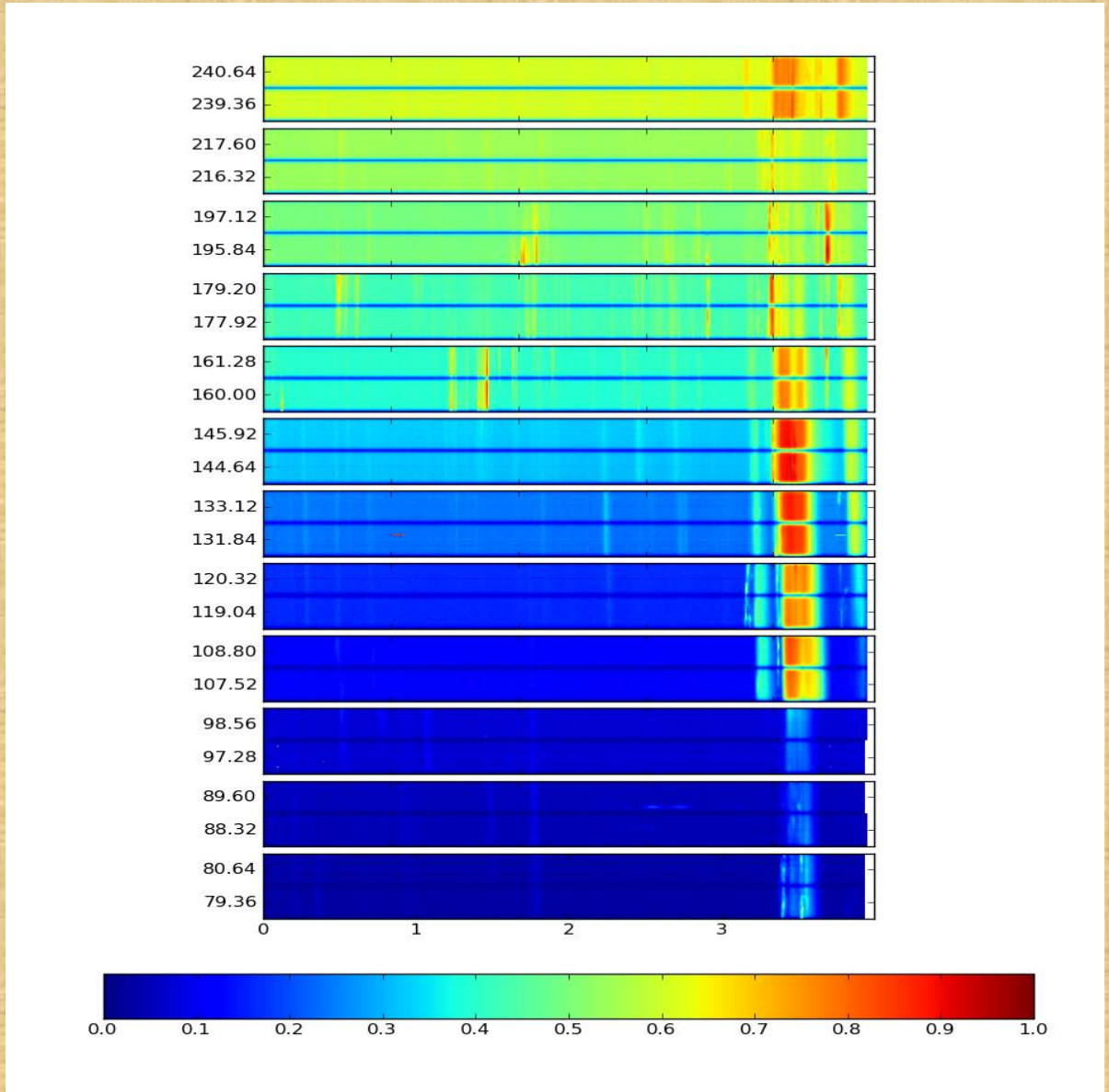
Imaging Dynamic Range
~5500


1082788696_13_14.160kHz.MS T1 T3 P0
14
12
10
8
6
4
2
0
0
100
200
300
400
0.252
0.248
0.244
0.240
0.236
0.232
0.228
0.224
0.220

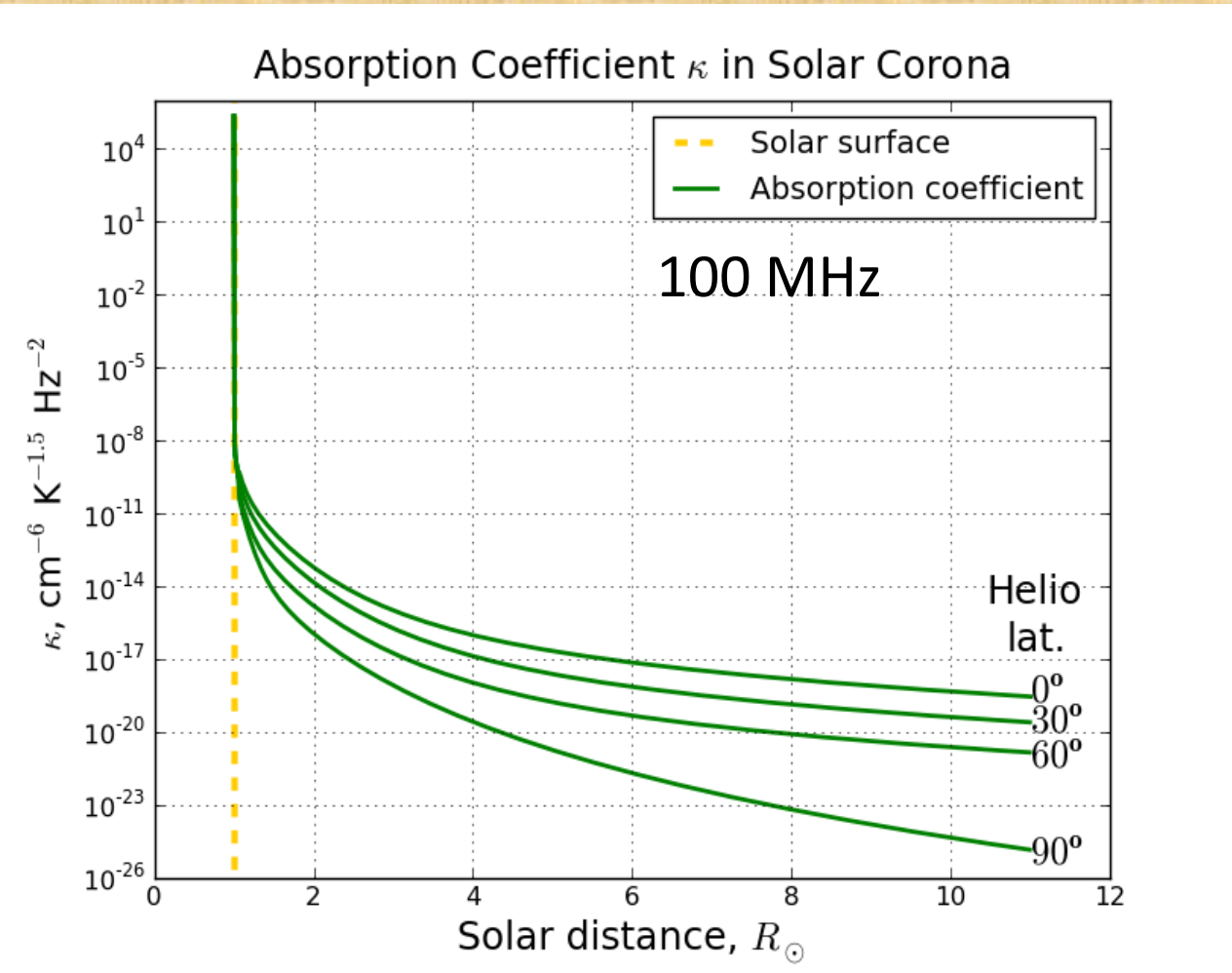
Partial Solar Eclipse (29 Apr, 2014)



Normalized cross correlations

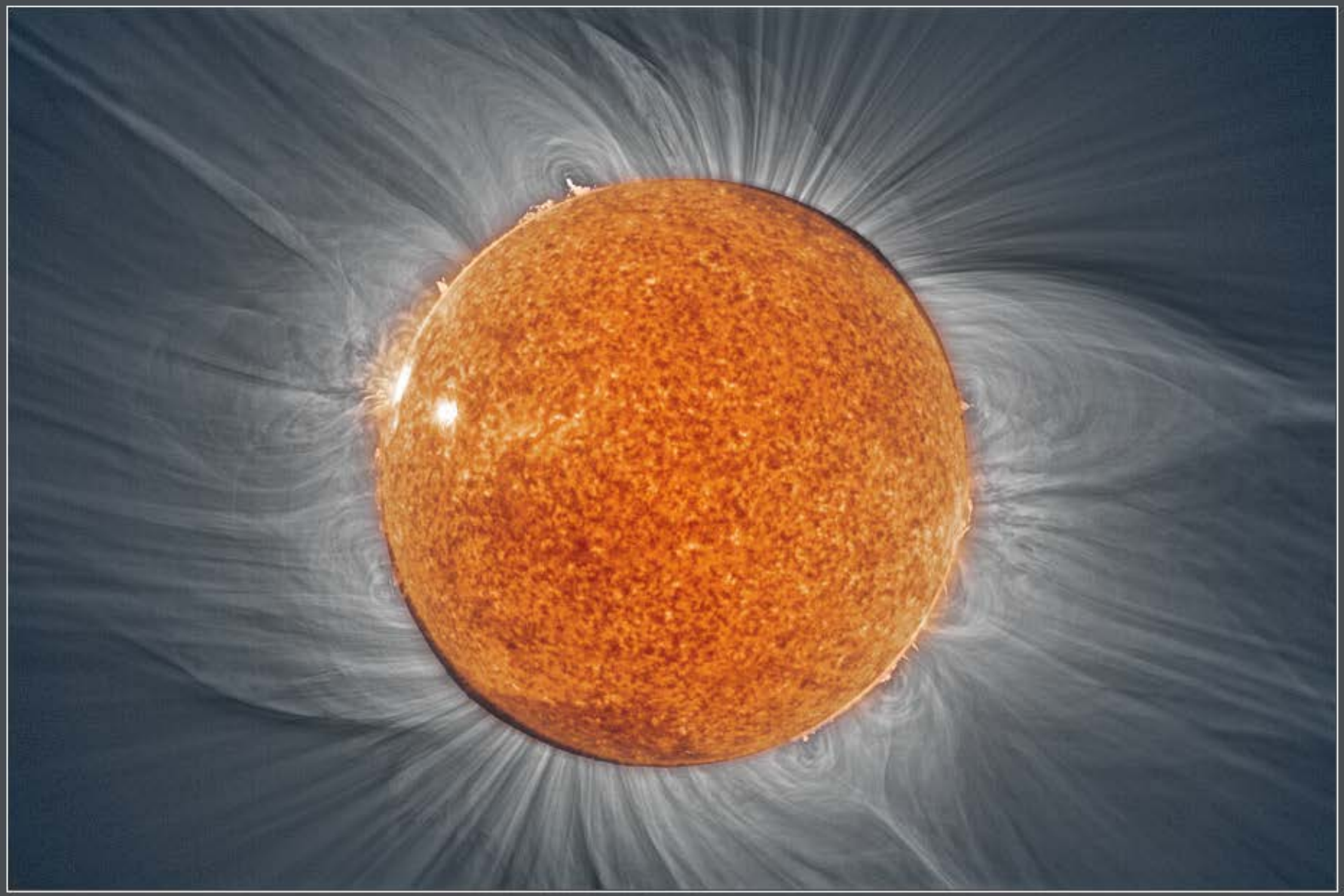


Variation of κ in the Chromosphere and Corona



$$\kappa = \frac{0.2\,N_e^{\,2}}{n\,T^{1.5}\,f^{2}}\;;$$

N_e and T_e are both strong function of radial distance from the Sun



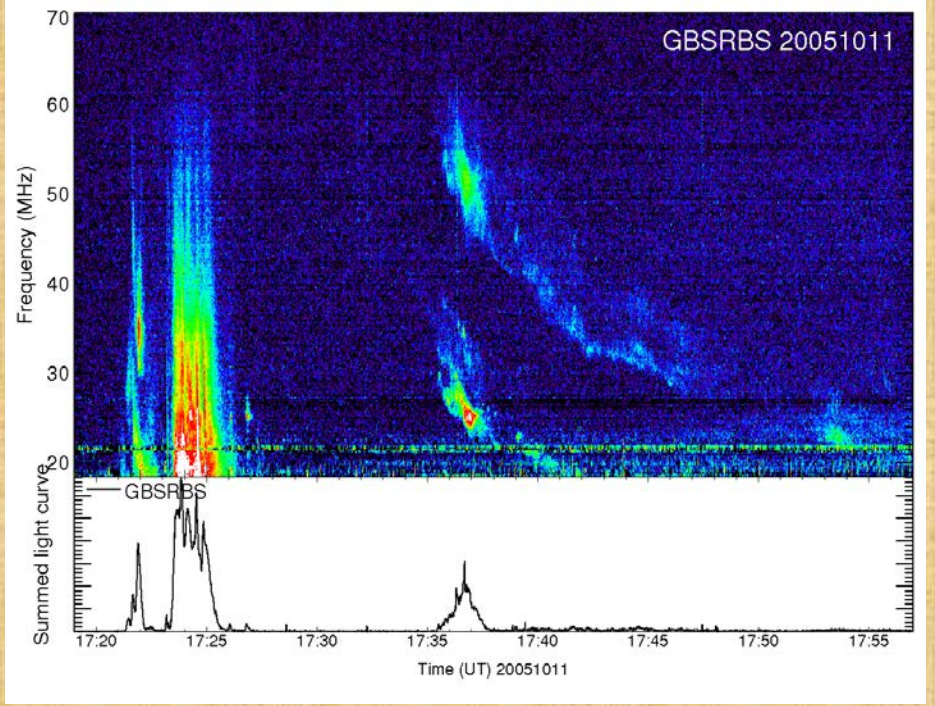
Total Solar Eclipse 2006

© 2006 Miloslav Druckmüller, Peter Aniol, ESA/NASA

Non-thermal Emission Processes

Plasma Emissions

- Non-linear conversion of electrostatic Langmuir waves to electro-magnetic waves
- Emission at local plasma frequency and its harmonic
- Responsible for Type II and Type III bursts
- Emission drifts from higher to lower frequencies

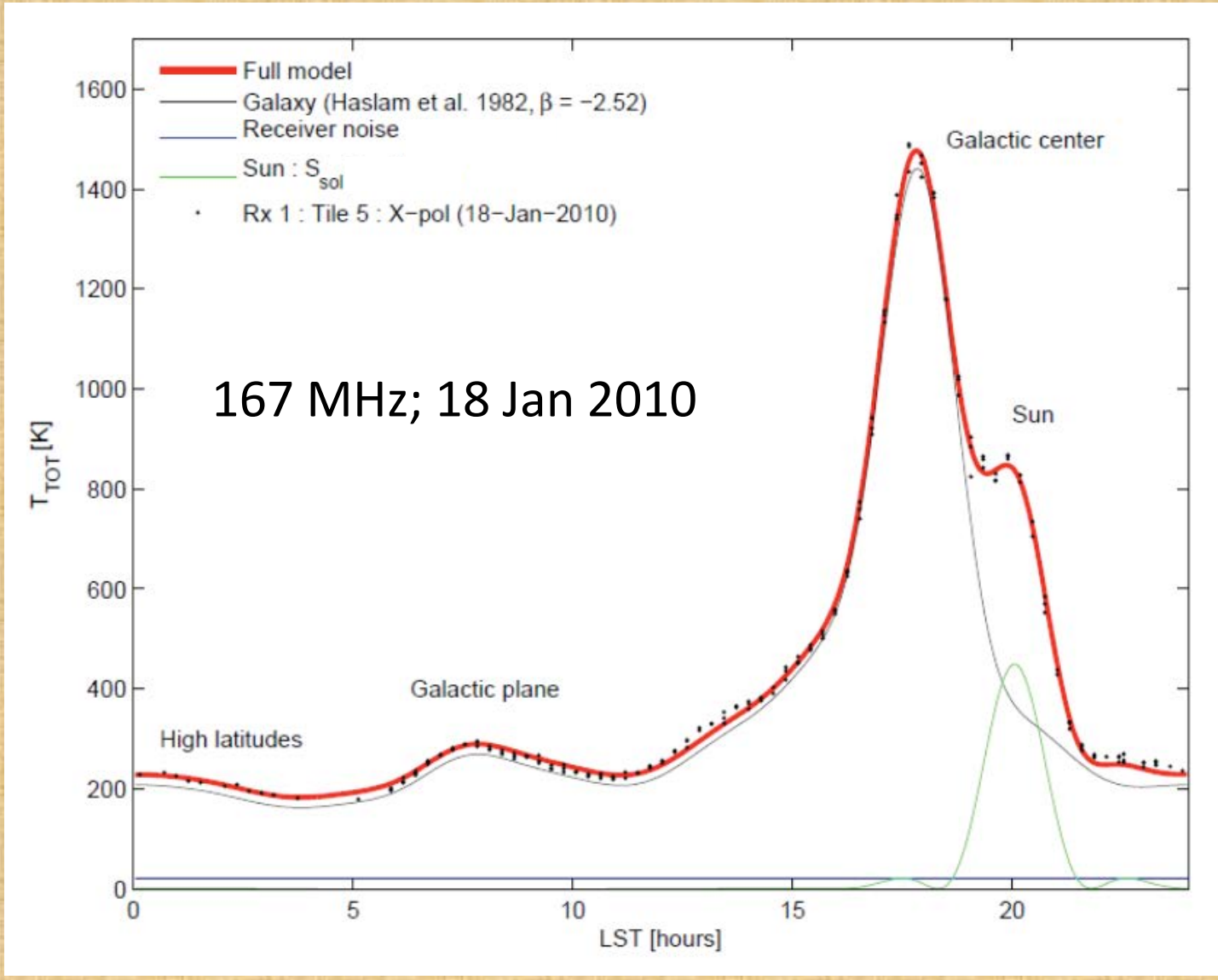


Brightness Temperatures (T_B)

Type III $10^6 – 10^9$ K

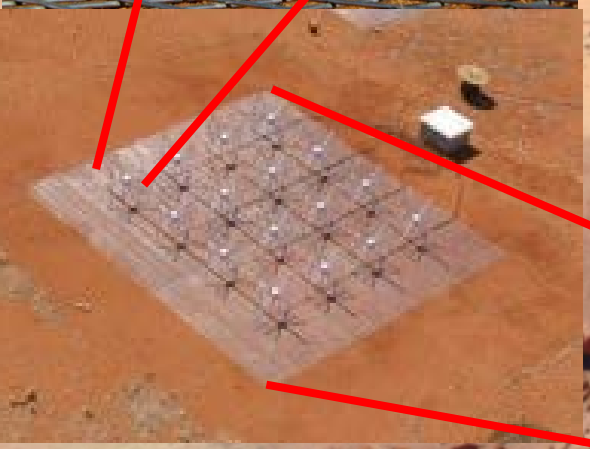
Type II $10^7 – 10^{12}$ K

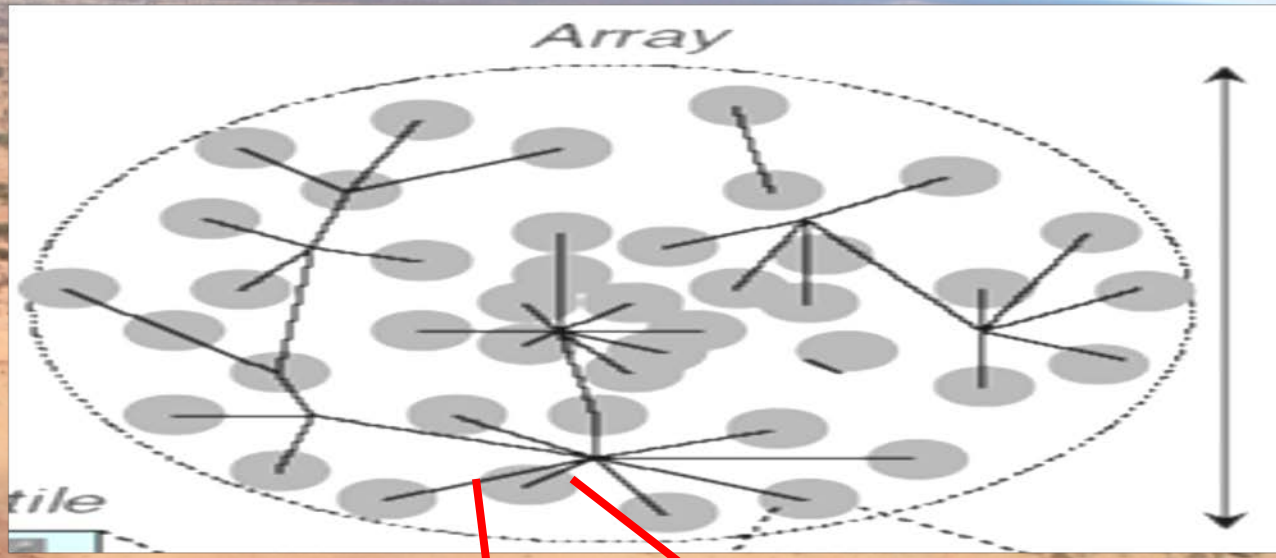
Zenith Drift scan

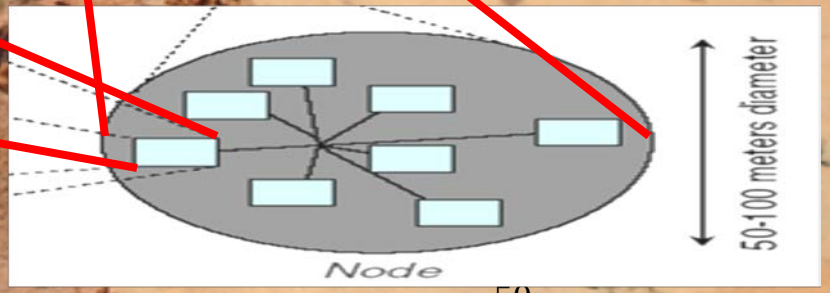


Murchison Widefield Array: Design









Some typical numbers

- MWA @ 150 MHz
  - $T_{SYS} = T_{REC} + T_{GAL}$ = 50 K + 350 K = 400 K (Tingay et al., 2013)
  - SEFD ~30 kJy (Feng, 2013, unpublished)
- Sun @ 150 MHz
  - B_{SUN} ~10^6 K (Brightness temperature of Sun)
  - S_{SUN} ~10^5 Jy $\Rightarrow$ T_{SUN} ~1300 K (Solar contribution to T_{SYS})
  - $T_{SYS} = T_{REC} + T_{GAL} + T_{SUN}$ = 1700 K
- Violate the usual RA assumptions
  - T_{SYS} dominated by T_{SRC}
  - Large normalised CCFs (0.1-0.6 even for the quiet Sun)
    - Van Vleck corrections become important